DESIGN AND CONSTRUCTION OF AXIAL SLOW FLOW CONTINUOUS WAVE FOLDED CARBON DIOXIDE LASER

A THESIS SUBMITTED TO
THE GRADUATE SCHOOL OF NATURAL AND APPLIED SCIENCES
OF
THE MIDDLE EAST TECHNICAL UNIVERSITY

BY

NECMETTİN KENAR

IN PARTIAL FULFILLEMENT OF THE REQUIREMENTS FOR THE DEGREE OF
MASTER OF SCIENCE
IN
THE DEPARTMENT OF PHYSICS

AUGUST 2003

Approval of the Graduate School of Natural and Applied Sciences

_____

Prof. Dr. Canan ÖZGEN
Director

I certify that this thesis satisfies all the requirements as a thesis for the degree of Master of Science.

_____

Prof. Dr. Sinan BİLİKMEN
Head of Department

This is to certify that we have read this thesis and that in our opinion it is fully adequate, in scope and quality, as a thesis for the degree of Master of Science

_____

Assoc. Prof. Dr. Gülay ÖKE
Superviser

Examining Committee Members

Prof. Dr. Sinan BİLİKMEN	_____
Assoc. Prof. Dr. Serhat ÇAKIR	_____
Assoc. Prof. Dr. Akif ESENDEMİR	_____
Dr. Ali ALAÇAKIR	_____
Assoc. Prof. Dr. Gülay ÖKE	_____

ABSTRACT

DESIGN AND CONSTRUCTION OF AXIAL SLOW FLOW CONTINUOUS WAVE FOLDED CARBON DIOXIDE LASER

KENAR, Necmettin
M.S., Department of Physics
Supervisor: Assoc. Prof. Dr. Gülay ÖKE

August 2003, 106 pages

Design and realization of a conventional carbon dioxide laser was performed. Gas composition and gas pressure effects on laser output power were studied. Effects of input electrical power and current on laser power were also investigated. Beam profiling of the laser beam was performed by pinhole method. Laser beam parameters like beam divergence, beam propagation factor were measured. These properties were extracted from focusing a laser beam in near field and performing a number of cuts across the beam cross-section and measuring the beam diameter at these points. Diameter measurements were obtained by knife edge method. Laser beam parameters were obtained for three different power laser beams in two axes across the beam. Found parameters were compared with regard to beam power and beam cross-section axis. Also possibility of using the obtained laser beam in material processing was investigated.

Keywords: Carbon dioxide laser, beam profiling, laser beam propagation factor.

ÖZ

YAVAŞ EKSENEL AKIŞLI SUREKLİ DALGA BÜKÜK KARBON DİOKSİT LASERİ TASARIM VE YAPIMI

KENAR, Necmettin
Yüksek Lisans, Fizik Bölümü
Tez Yöneticisi: Doç. Dr. Gülay ÖKE

Ağustos 2003, 106 sayfa

Geleneksel karbon dioksit laseri tasarımı ve gerçekleştirilmesi çalışması yapılmıştır. Gaz karışım oranlarının ve gaz basıncının laserin çıkış gücü üzerine etkileri çalışılmıştır. Elektrik giriş gücü ve akımının laserin gücü üzerine etkileride ayrıca incelenmiştir. Laser demeti kesitinde üç boyutlu güç şiddeti profili iğne deliği yöntemiyle çıkartılmıştır. Laser demeti parametreleri , demet genişleme ve demet yayılma katsayısı ölçülmüştür. Bu özellikler yakın mesafede laser demeti odaklanarak, demetten çok sayıda kesit alınarak ölçülen demet çaplarından çıkartılmıştır. Çap ölçümleri bıçak kenarı yöntemi ile yapılmıştır. Laser demet parametreleri üç ayrı güçte laser demetinin her iki kesit ekseni için elde edilmiştir. Bulunan parametreler demet gücü ve eksen açısından değerlendirilmiştir. Ayrıca elde edilen laser demetinin malzeme işlemede kullanılma imkanları araştırılmıştır.

Anahtar Kelimeler: Karbon dioksit laseri, laser demeti güç şiddeti profili, laser demeti yayılma katsayısı.

In Memory of Dr. Iulian GUTU

ACKNOWLEDGEMENTS

I would like to express my sincere thanks to my advisor Assoc. Prof. Dr. Gülay ÖKE for her support and careful reading of manuscript.

I would like to express my sincere thanks to Prof. Dr. Sinan BİLİKMEN for the opportunity to study on CO_2 lasers as a member of Laser Laboratory.

I am very grateful to late Dr. Iulian GUTU for the discussions on CO_2 lasers and laser material processing. He was the person who established my basics on the subject.

I am grateful to Dr. Ali Alacakır for tolerating my faults and his help during experiments.

I am also grateful to Mr. Oğuz PERVAN for his encouragement and help during experiments.

I thank to Dr. Hilal GÖKTAŞ for allowing me to use his instruments.

Special thanks go to İlker YILDIZ and Ertan ERYILMAZ for their friendship and help during my work.

I express my thanks to our technicians İsmail DOĞRU, Muharrem KUZU and Murat AYDIN for their help.

I would like to thank to Mr. Semih ÖZEL from Genel Makina Tasarım Ltd. Şti. for manufacturing of beam delivery unit and 3-axis stage, without his kind help this work could not be completed.

I would like to thank to Mr. Hikmet ÖZGÜR from Makina Dizayn Ltd. Şti. for spending his valuable time in supplying material that I could not find,

Also I thank to Mr. İbrahim DİNÇER from Dinçer Medikal Ltd. Şti. for his valuable discussions and encouragement.

At last but not least I would like to express my sincere thanks to my family for their patient and support during my work.

TABLE OF CONTENTS

LIST OF TABLES

TABLE

LIST OF FIGURES

FIGURES

CHAPTER 1

INTRODUCTION

In the world of high speed technological development, lasers as general take their place on top of the subjects studied in the last 40 years. The needs of industry force the research and development of lasers. Lasers especially that with high power have wide application areas in manufacturing industry. Their main application areas are cutting (about %80), welding, heat treatment, alloying and cladding. In these manufacturing areas the use of CO_2 and Nd:YAG lasers is dominated. Since the developments in solid state lasers in the last ten years increase their use in manufacturing market, but still CO_2 lasers are widely used and technological developments in CO_2 laser fixes their application areas in the market. CO_2 lasers are still cheap and have better beam properties than solid state lasers and this makes them worth to work on.

In our country very little work on CO_2 lasers is done and needs of our market for cheap and powerful lasers was the main reason of this work. The lack of experience in this area force us to start with the basic laser design structures. Also need of practical methods for determining the beam properties of a powerful laser beam oriented us to use basic methods such as pinhole and knife edge techniques. The manuscript text of the work was prepared in such an order first to give basics of CO_2 lasers than their theory and than to pass to basic design needs according to which design calculations are made. After the design calculations the realization of the design was described and experiments carried out were discussed.

In Chapter 2, main design criteria of slow flow axial laser is given and background covering the engineering and technical aspects of laser design was tried to be established.

In Chapter 3, having in hand some experimental results and technical considerations obtained from Chapter 2, theoretical background of CO_2 lasers is given and the physics of CO_2 lasers is established in connection with macroscopic phenomena taking place in lasers.

Chapter 4 introduces beam properties of lasers and connects these properties to the mechanical design of laser. Also focusing of a laser beam and some results that may effect the processing are described.

In Chapter 5, design method and calculations are extensively described and results that were considered in the mechanical realization of the design are given.

In Chapter 6 experiments carried out on the realized design are described and obtained results are discussed. In this chapter gas concentration and pressure effect on lasing, beam profiling, beam propagation factor estimations and possible material processing applications are given.

Calculations carried out during the work, some technical drawings, photos and description of used techniques are left for Appendices.

CHAPTER 2

FUNDAMENTALS OF CO_2 LASER

2.1-History

Infrared radiation emission from CO_2 was first reported by Patel [1] in 1964 in pulsed discharge through pure CO_2. Soon after that it had been realized that a much more efficient system involving the vibrational energy transfer from N_2 to CO_2 was possible. Such a laser had been build by Patel [2] also in the same year. This laser incorporates the RF excitation of N_2 molecules, which are then injected to the CO_2 gas.

In these studies output powers of continuous wave (cw) operating CO_2 lasers were between 0.1 mW to 200 mW. The addition of N_2 increased the efficiency of the CO_2 laser from 10^{-6} to 10^{-3}. Direct excitation of a flowing N_2 and CO_2 gas mixture using a dc discharge was found to yield cw power of 11.91 W with efficiency of ≅ 3 % by Patel [3].

Another major advance occurred when the addition of He was found to increase the cw power obtainable from a flowing N_2, CO_2 gas mixture to 106 W [4].

The efficiency of this system was less than 6%. The theoretical efficiency of the CO_2 laser operating at a wavelength of 10.6 μm was predicted to be ≅ 40 % and at these years the efficiencies obtained were far away the theoretical limit. In 1967 a

162-ft long cw CO_2 laser had been built and operated at a power output of 2.3 kW [5]. Subsequently, the development of electric discharge convection and gas dynamic lasers has resulted in generation of cw laser powers in excess of 100 kW. But the size of these lasers was not convenient for industrial purposes.

The year 1969 marked a turning point in the development of high-power cw and pulsed CO_2 lasers. Late in 1969, Beaulieu [6] reported that CO_2 laser emission could be obtained at atmospheric pressure and above by exciting the gas transversely so that the discharge passed perpendicular to the optical axis. This has led directly to devices that rely on the creation of high densities of electronic charge using electron beam excitation [7] or volumetric photoionization [8] independent of the discharge that is used to excite laser emission. As a result Q-switched CO_2 lasers were developed.

In the same year development of lasers based on convective cooling [9], [10] were realized and a report was published describing the operation of a compact closed system cw laser using rapid transverse gas flow capable of generating powers of 1 kW [11].

Theoretical development of CO_2 laser was completed in 10 years after its invention. Through the proceeding years works on these lasers were concentrated on development of new excitation mechanisms, new resonator types and more efficient laser optics.

2.2- Slow Axial Flow CO_2 Laser

Slow axial flow lasers are no more ‘state of art’ lasers. Main difference from the other types of lasers is that; cooling mechanism is diffusion and gas flow rate is maximum 50 cm^3/min.

2.2.1 – General Design

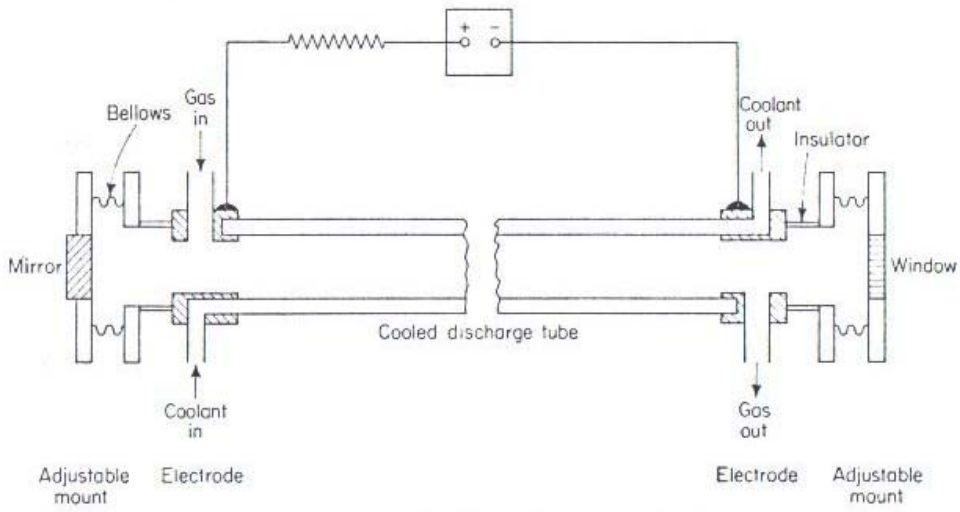

Figure 2.1- Schematic diagram of a conventional CO2 Laser

A laser primarily consists of the following parts; two mirrors one total reflector and the other partial reflector, a tube used as chamber and anode-cathode pair. Gas mixture flows in the tube between anode and cathode. During this flow the gas mixture is excited and as a result of this excitation photons are obtained. Photons travel between the two mirrors by exciting the gas again and increasing the number of photons in the cavity. Through the output mirror, which allows photons to escape out of the cavity, a laser beam is obtained. ***Fig. 2.1*** shows the general sketch on conventional CO_2 laser.

The laser tube is enclosed by a coolant (water, oil etc.) jacket, by which the excess heat in the cavity is removed. Cooling of the cavity is of great importance to the operation of the laser as going to be discussed below.

2.2.2- Gas composition and Gas Flow

First lasing from CO_2 laser was obtained from pure CO_2 gas. But the output power obtained was very low. Subsequent addition of N_2 and He increased output power very much. ***Fig. 2.2*** shows the effect of different gas compositions on laser gain.

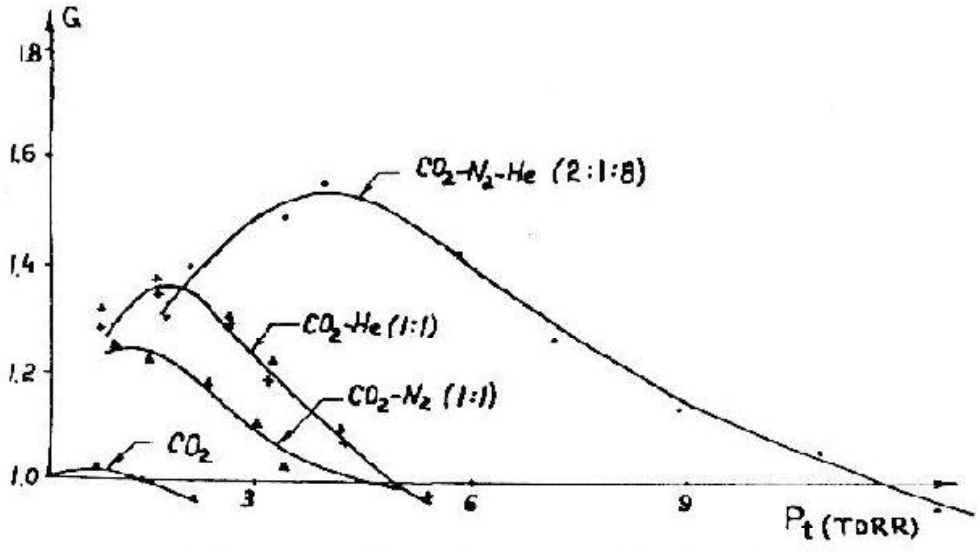

Figure 2.2- Gain versus total mixture pressure [12]

As it can be seen from the figure, CO_2 alone has very low power gain. This is due to the inefficient electrical excitation made directly to CO_2 gas. Addition of N_2 increased the laser gain by factor of 10. This is a result of the efficient excitation of N_2 and that nitrogen has a very long-lived first-excited vibrational state that almost exactly matches the upper level of CO_2. The energy transfer between the N_2 and CO_2 molecule is very efficient as a consequence of the close energy levels. The graph

showing the vibrational energy levels of CO_2 and N_2 and the excitation mechanism of CO_2 laser are shown in ***Fig. 2.3.***

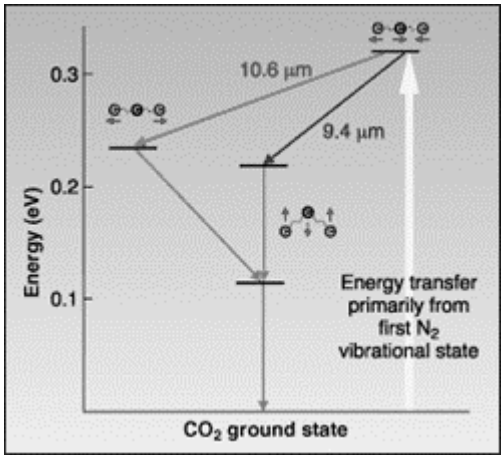

Figure 2.3- Excitation Mechanism of CO_2 Laser [13]

From ***Fig. 2.3*** we can see that He has no effect in the excitation of CO_2 but addition of it to pure CO_2 or to CO_2-N_2 mixture increases power gain very much. This can be explained by the high heat transfer coefficient of He gas compared with CO_2 and N_2.

Gain in CO_2 laser is not only a function of gas composition but also it is a function of gas flow rate. In ***Fig. 2.4*** it is shown that with an increase in flow rate gain of a given laser increases first and then saturates after a given flow rate depending on tube diameter. But the saturation of gain does not mean an obtainable constant power. Power can increase after that point but very slowly. The primary effect of flowing gas on gas discharge is a reduction of gas temperature by convection, where as in slow flowing gases the heat transfer is obtained by diffusion.

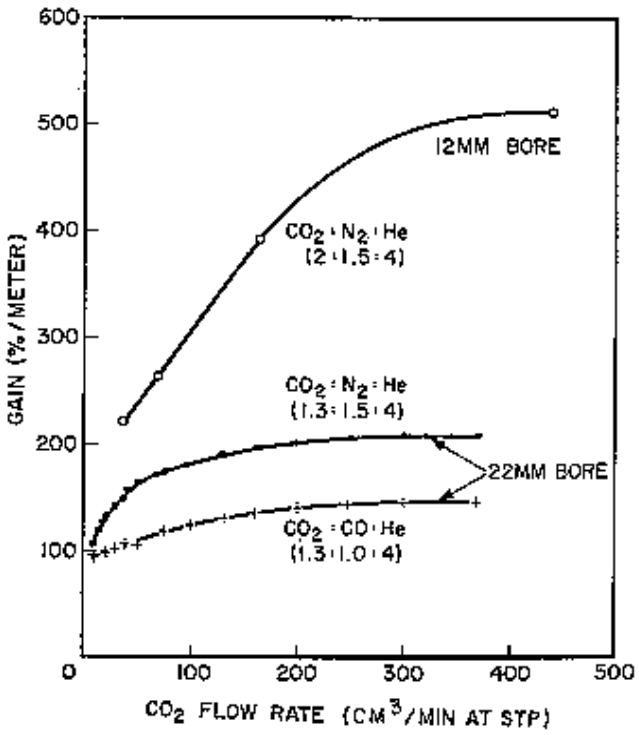

Figure 2.4- Gain versus CO_2 flow rate for CO_2:N_2: He mixture at near optimum pressure and mixture ratio [14]

2.2.3- Tube Diameter

Gain of a laser is a function of tube diameter also. ***Fig. 2.5*** depicts a usual dependence of gain on tube diameter. Gain decreases with increasing tube diameter. Although this situation cannot be explained very simply, there are three effects which are produced with the decrease of tube diameter. First, by decrease in tube diameter an increase in longitudinal field is observed. This increase in the field leads to increase in electron temperatures that imply an increase in electron energy. This leads to increase in pumping rate and gain coefficient. Second, if the volume pump rate is constant decrease in tube diameter results in increase in the gas velocity that causes a faster gas exchange. Therefore, during the passage of the gas through the

tube, decomposition of CO_2 decreases and gain increases. Third, with the decrease in tube diameter the temperature difference between the gas center and the tube walls decreases, That is, heat removal from the gas is enhanced and the gain is increased.

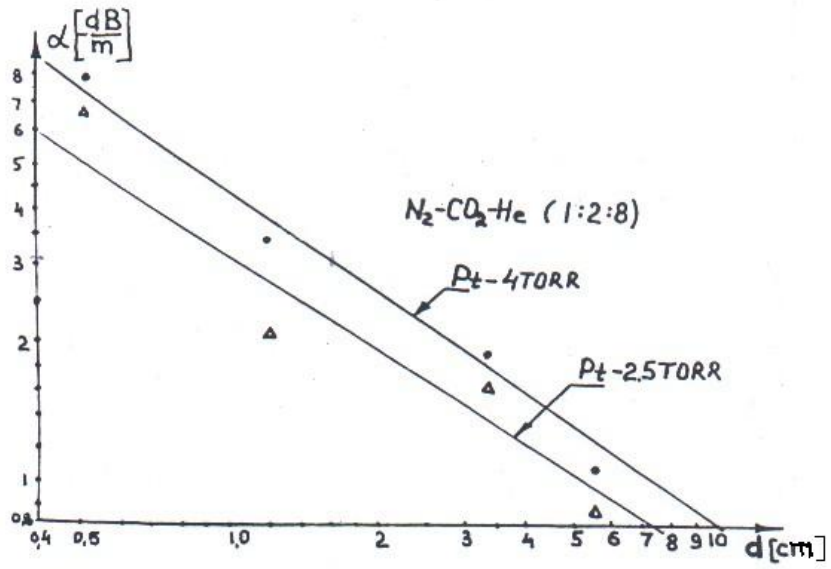

Figure 2.5- Gain versus tube diameter for optimum current density [12]

2.2.4- Pressure and Current

As it is clear from ***Fig. 2.2*** gain is also a function of pressure. For a given gas mixture gain increases with increasing pressure. This is an expected result since density of CO_2 and N_2 molecules increases giving rise to gain. However, with increasing pressure, field intensity is growing as a result of which input energy in the gas and gas temperature are increased resulting in a decrease in the gain. So, for each gas mixture there exists an optimum pressure for which maximum gain is obtained.

In condition of optimum gas mixture and constant flow rate the dependence of gain on current is depicted in ***Fig. 2.6***. Here increase in current means increase in input power which is expected to increase gain of the amplifier. But increase in input power results in excess power stored in gas medium which in consequence increases gas temperature. Increase in gas temperature as mentioned above means decrease in amplifier gain. Also from ***Fig. 2.7*** it can be seen that optimum current is also dependent on tube diameter.

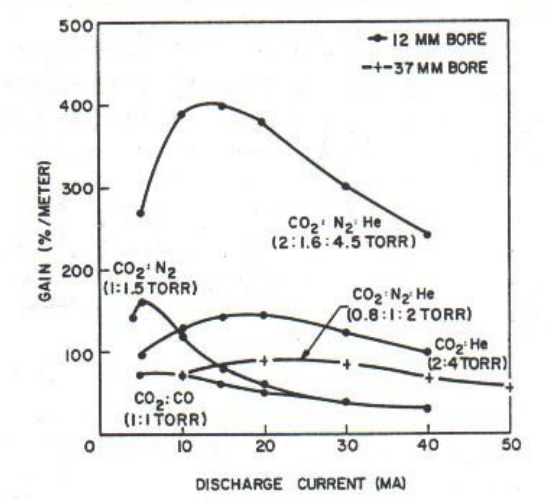

Figure 2.6- Gain versus discharge current for various flowing gas media at optimum mixture ratios and a constant flow rate in 12 and 37 mm bore amplifier tubes [14]

2.2.5- Discharge Energy and Gas Temperature

Gas temperature plays a key role in gas laser excitation. It depends on input energy density having a scaled unit of Joule/(Volume x Pressure). In the discharge tube gas temperature has a radial gradient. That is temperature is high at the center of. the tube and decreases gradually to the tube wall.

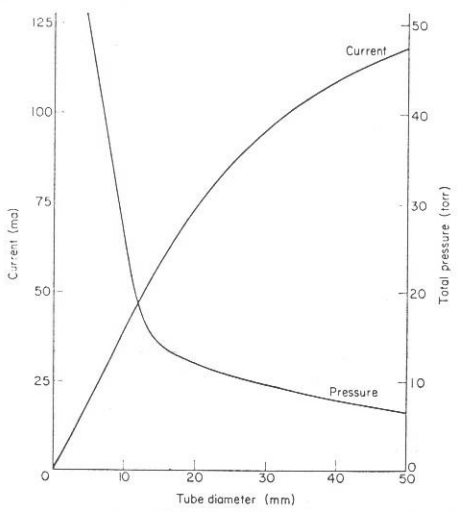

Figure 2.7- Optimum current and total pressures for maximum cw oscillator output power as a function of tube diameter [15]

Fig. 2.8 depicts the behavior of gas temperature and small signal gain in discharge tube for two different input energies From ***Fig. 2.8*** we can conclude that at small input energies the gain distribution reflects the input energy distribution. However as the input energy increases after a certain energy input value the gain distribution does not continue to reflect the spatial energy input distribution. The temperature of the gas at the center of the tube increases and the gain starts to decrease.

The spatial energy distribution posses the same profile as shown in ***Fig. 2.9*** but gain profile is changing in not preferred way. The decrease of gain is not a direct function of temperature increase. Increased temperature increases the dissociation of CO_2 and the increase in content of CO decreases gain of the medium. Carbon-monoxide production rate as a function of input energy distribution is shown in ***Fig. 2.10***. The CO production is directly proportional to the discharge energy.

In ***Fig. 2.11*** the dependence of gain and gas temperature on input energy is shown. Temperature increase is a direct function of energy input. But gain has a maximum at certain temperature or input energy and after that point it starts to decrease.

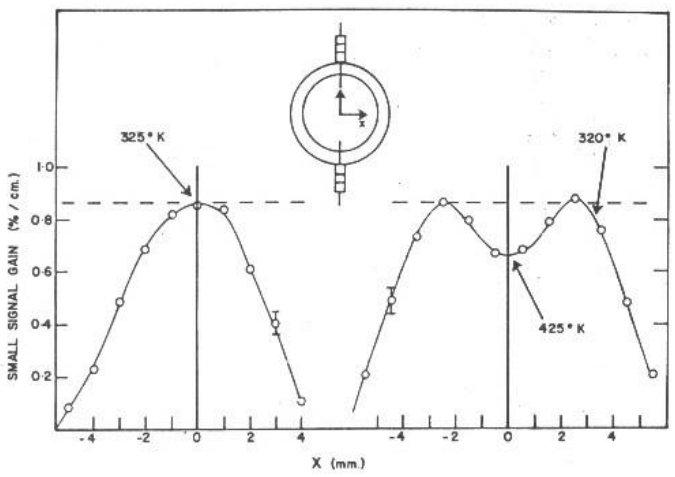

Figure 2.8- Spatial variation of gain for a 3% CO_2: 10%N_2: 87% He mixture at 100 torr. Two gain distributions are shown; the one on the left corresponds to an energy input of 120 J/l atm. The other gain distribution corresponds to an input energy of 350 J/l atm. Representative gas temperatures are also shown [16]

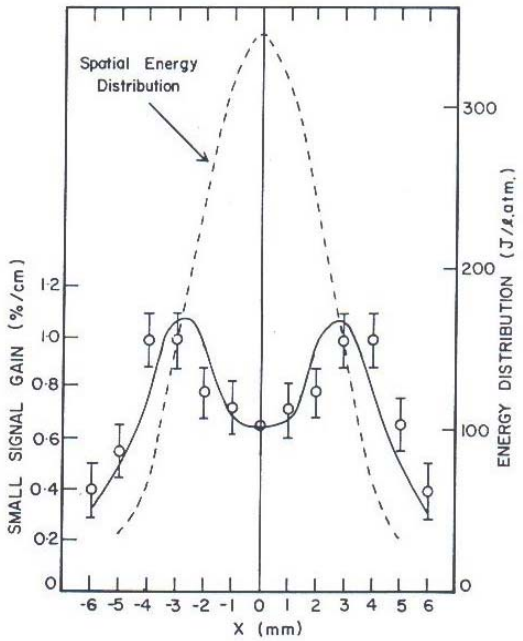

Figure 2.9- Spatial variation of gain for a 10%CO_2: 90% He mixture at 150 Torr [16]

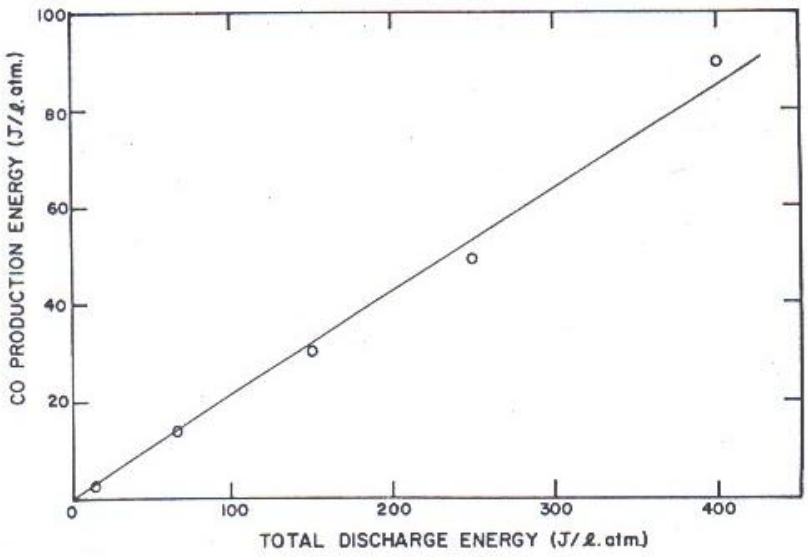

Figure 2.10- Carbon-monoxide production in a 10%CO_2: 90% He mixture at 150 Torr [16]

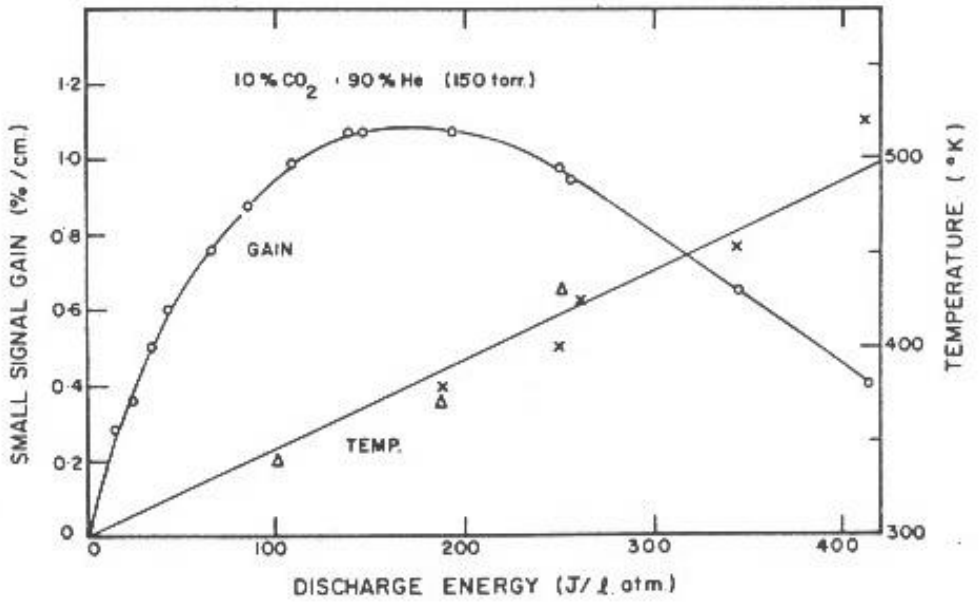

Figure 2.11- Small-signal gain and gas temperature as a function of energy [16]

2.2.6- Resonator Configuration and Output Coupling

Generally a resonator is consisting of a discharge medium and two mirrors. Mirror configurations may vary in regard to their curvature and resonator length. Possible resonator configurations are given in ***Fig. 2.12***. Selection of resonator is a question of application. Usually the end mirror is fully reflective. Materials for end mirror are Au, Ag coated Cu, Mo and Si. Curvature of the mirror is determined by the desired output beam characteristics and stability criteria of the resonator.

The most important issue in laser design is determination of the reflectivity or transmission of the output mirror. Less transmission of the output mirror means obtaining less power from that a resonator can give. However, large transmissions decrease photons that sustain the laser action in the resonator cavity so obtained power also decrease. The effect of transmission of the output mirror on the obtained laser power is given in ***Fig. 2.13***. Here the effect of output coupling mentioned above can be seen clearly. So an optimum value for the transmission of output mirror should be chosen. In his report Tyte [15] gives a graph from which an optimum reflectivity for the output mirror can be chosen with respect to resonator length/discharge tube diameter. This graph is given in ***Fig. 2.14.*** The graph is based on experimental values and it is difficult to obtain desired results using it.

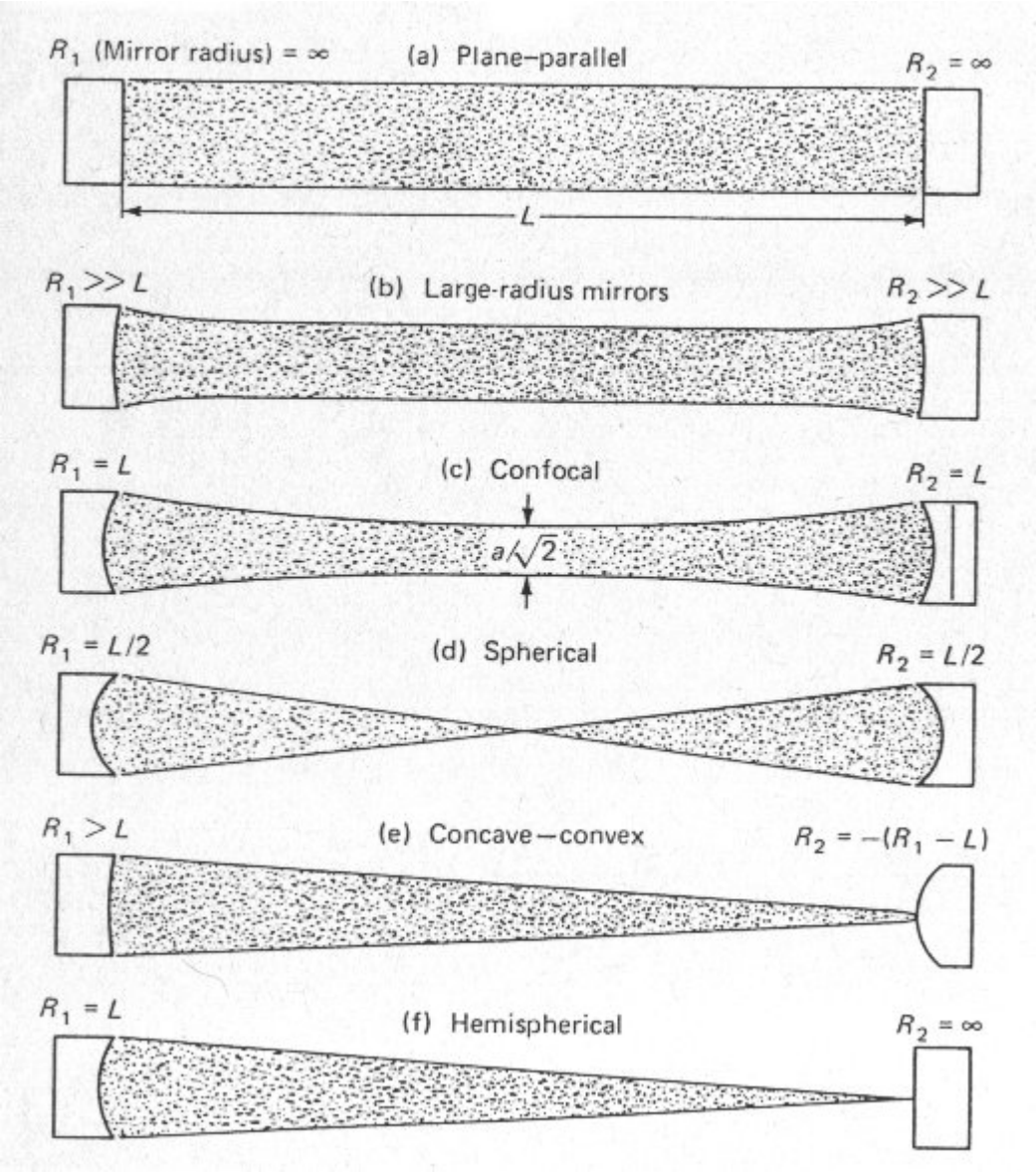

Figure 2.12- Resonator Configurations

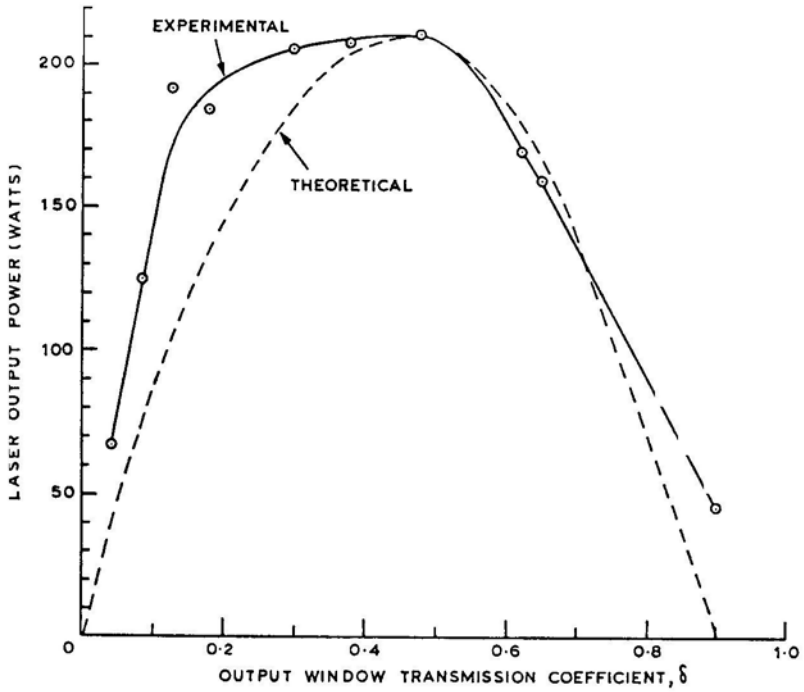

Figure 2.13- Graph of output power versus window reflectivity [15]

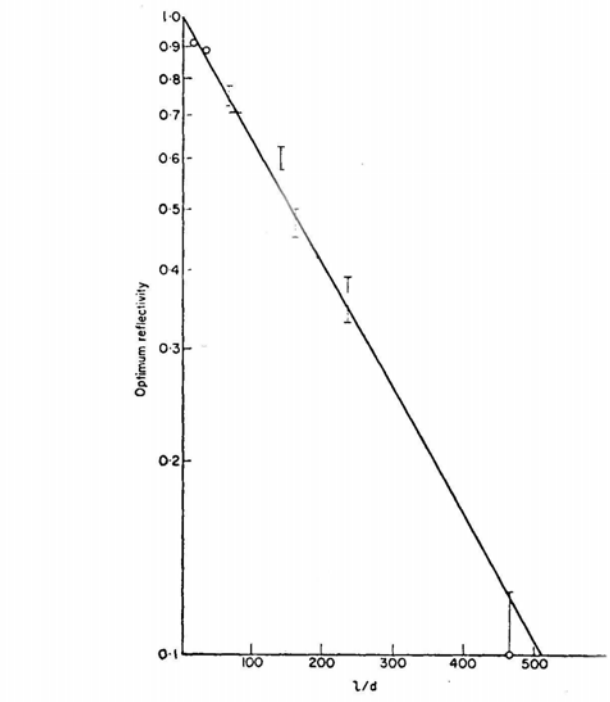

Figure 2.14- Optimum reflectivity as a function of the ratio of laser length to diameter [15]

Since each amplifying medium is defined by its saturation intensity and small signal gain a relation to obtain optimum output transmission should include these parameters beside the resonator length and diameter. Such a relation is given by Rigrod [17]. This relation includes reflectivities of both mirrors, resonator length, discharge cross section, small signal gain and saturation intensity. The formula is:

$$P = \frac{r_1^{1/2} t g_o I_s S}{\left[r_1^{1/2} + r_2^{1/2}\right]\left[1-(r_1 r_2)^{1/2}\right]}\left[L + \frac{\ln(r_1 r_2)}{2g_o}\right] \tag{2.1}$$

where P is the output power, r_1 and r_2 are the reflectivities of end and output mirror respectively, t is transmission of output mirror, S is cross section area, I_s is saturation intensity, g_o is small signal gain and L is discharge length. From this formula by taking out $P_{av}=g_o I_s V$ which is the available power in the resonator we obtain a formula for efficiency like

$$\eta = \frac{P}{P_{av}} = \frac{r_1^{1/2} t}{\left[r_1^{1/2} + r_2^{1/2}\right]\left[1-(r_1 r_2)^{1/2}\right]}\left[1 + \frac{\ln(r_1 r_2)}{2g_o L}\right] \tag{2.2}$$

Using this equation we can obtain a plot of efficiency versus transmission for the output mirror. From the plot transmission value giving the highest efficiency is selected to be the transmission of the output mirror. In this formula also there is an unclear part; how can g_o be determined. There are two ways to found g_o: one by measuring it, which is the long way and second by taking it from graphs such as ***Fig. 2.5***. From equation (2.2) it is clear that output transmission is a function of mirror reflectivities and g_oL product. Only one parameter is experimental the others are given.

CHAPTER 3

THEORY OF CO_2 LASER

3.1 – Carbon Dioxide Molecule

Carbon dioxide is a linear, symmetric, triatomic molecule. This molecule can vibrate in the three independent modes of vibration shown in ***Fig. 3.1***. They are: the longitudinal symmetric mode in which the carbon atom remains stationary and the oxygen atoms move in opposite directions along the line of symmetry; the bending mode in which the atoms all move in a plane perpendicular to the line of symmetry, the carbon going one way while the two oxygen go the other; and the asymmetric mode in which the atoms all move along the line of symmetry, the carbon moving in the opposite direction to the two oxygen atoms. Each of these modes is characterized by a definite frequency of vibration. According to basic quantum mechanics these vibrational degrees of freedom are quantized, that is when a molecule vibrates in any of the modes it can have only a discrete set of energies. Thus if we call ν_1 the frequency corresponding to the symmetric mode then the molecule can have energies of only

$$E = \left(n + \frac{1}{2} \right) h\nu_1 , \qquad \text{n= 0,1,2,...} \tag{3.1}$$

when it vibrates in the symmetric stretch mode. Thus the degree of excitation is

characterized by the integer *n* when the carbon dioxide molecule vibrates in the symmetric stretch mode. In general, since the carbon dioxide molecule can vibrate in a combination of the three modes the state of vibration can be described by three integers (*nmq*); the three integers correspond respectively to the degree of excitation in the symmetric, bending and asymmetric mode. ***Fig. 3*** also shows the different vibrational energy levels taking part in the laser transition. The laser transition at 10.6 μm occurs between the (001) and (100) levels of carbon dioxide.

The CO_2 energy levels, which are of greatest importance in laser action, are situated 2349.3 cm^{-1}, 1388.3 cm^{-1}, 1285.5 cm^{-1} and 667.3 cm^{-1} above the ground state.

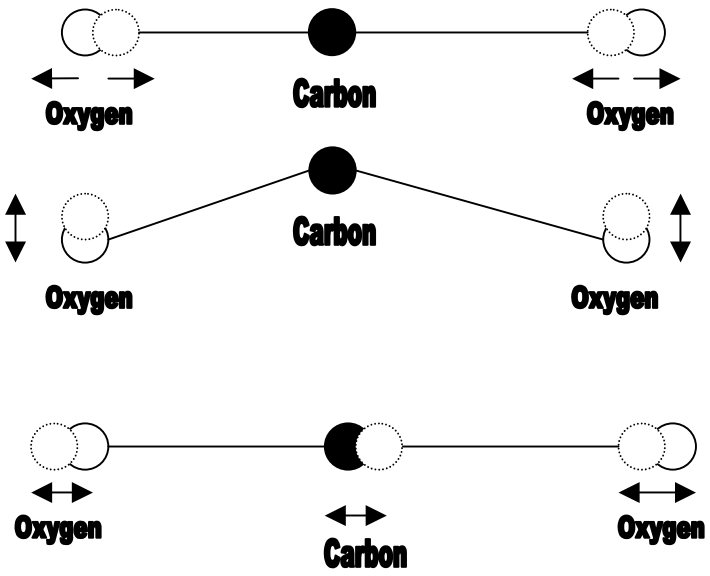

Figure 3.1 - The fundamental modes of vibration of the CO_2 molecule

3.2- Excitation of Carbon Dioxide

The excitation of the carbon dioxide molecules to the long lived level (001) occurs both through collisional energy transfer from nearly resonant excited nitrogen molecules and also from the cascading down of carbon dioxide molecules from higher energy levels.

The first vibrationally excited level of N_2 lies 2329.66 cm^{-1} above the unexcited ground state. The (001) level of CO_2 is 20 cm^{-1} above the first excited level of N_2. Thus energy can be transferred between N_2 and CO_2 with high efficiency when N_2 collides with CO_2. The transfer equation is given by

$$N_2(v``=1) + CO_2(000) \leftrightarrow N_2(v``=0) + CO_2(001) - 18\ cm^{-1} \qquad (3.2)$$

and the rate of energy exchange is $k=1.9x10^4$ Torr/sec at 300 ^oK [18].

3.3- Relaxation Process

Early in the development of CO_2 lasers, it was realized that adding He in quantity to the laser gas resulted in substantially increased output powers. It is now established that the primary effect of He is to relax the lower laser level while essentially unaffecting the population in the (001) state. Furthermore, He is also effective in depopulating the (010) level and may also lower the gas kinetic temperature. All these effects are beneficial to high power laser operation, since a radiative relaxation rates are orders of magnitude smaller than those due to collisions with He atoms and other gaseous components.

Quenching process involving the (010) level include the vibrational-translational energy transfer

$$CO_2(01^10) + M \rightarrow CO_2(00^00) + M + 667\ cm^{-1} \quad (3.3)$$

The relaxation of the two lower laser levels $(10^00,02^00)_I$ and $(10^00,02^00)_{II}$, these levels correspond to levels with energies of 1388.3 cm^{-1} and 1285.5 cm^{-1}, may occur through

$$CO_2(10^00,02^00)_I + CO_2(00^00) \leftrightarrow 2CO_2(01^10) + 64\ cm^{-1} \quad (3.4)$$

$$CO_2(10^00,02^00)_{II} + CO_2(00^00) \leftrightarrow 2CO_2(01^10) - 40\ cm^{-1} \quad (3.5)$$

or $(1000,0200)_I$ may relax via the process (Tyte [15])

$$CO_2(10^00,02^00)_I + CO_2(00^00) \leftrightarrow CO_2(02^20) + CO_2(00^00) + 52.7\ cm^{-1} \quad (3.6)$$

$$CO_2(02^20)_I + CO_2(00^00) \leftrightarrow 2CO_2(01^10) + 1\ cm^{-1} \quad (3.7)$$

Rate constants associated with these processes depend on temperature, pressure, and type of quencher. Lifetimes associated with the states involved in excitation and relaxation is shown in ***Fig. 3.2.***

3.4- General Energy Transfer Processes in CO_2 Laser

Of the many energy-transfer processes, which occur in CO_2-N_2-He laser mixture, the following equations (which also include the ones given above) are found to be the most important and are given by Fowler [19];

i) Electron excitation and deexcitation of the CO_2 asymmetric stretch mode,

$$e + CO_2[l,m,(n-1)] \leftrightarrow e + CO_2(l,m,n), \quad (3.8)$$

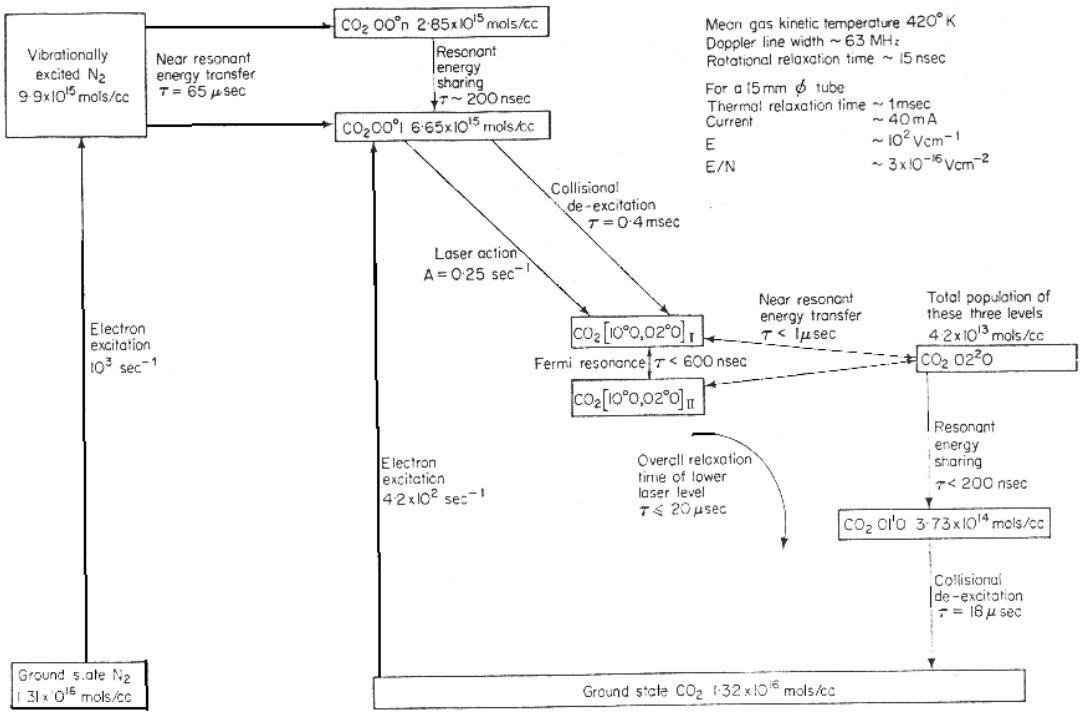

Figure 3.2- Schematic diagram of the CO_2 laser mechanism showing relaxation times for typical gas mixture (1:1:8 of CO_2:N_2:He) at a total pressure of 15 torr and a gas-kinetic temperature of 420 ^oK. Level populations shown are equilibrium vibrational populations in the absence of laser action [15].

ii) Vibrational energy exchange between N_2 and the asymmetric stretch mode of CO_2,

$$N_2(v) + CO_2\,[l,m,(n-1)] \leftrightarrow N_2(v-1) + CO_2\,(l,m,n), \tag{3.9}$$

iii) Vibrational energy exchange between the asymmetric stretch and the coupled symmetric stretch and bending modes of CO_2,

$$M + CO_2\,[l,m,(n-1)] \leftrightarrow M + CO_2\,[(l-1),\,(m-1),\,n], \tag{3.10}$$

iv) Electron excitation and deexcitation of N_2,

$$e + N_2(v) \leftrightarrow e + N_2\,(v'), \tag{3.11}$$

v) Excitation and deexcitation by both electrons and heavy particles of the bending mode of CO_2,

$$M + CO_2[l,(m-1),n] \leftrightarrow M + CO_2[l, m, n], \quad (3.12)$$

vi) Absorption and spontaneous emission of 4.3 μm radiation by CO2,

$$CO_2[l,m,(n-1)] + \text{photon (4.3 μm)} \leftrightarrow CO_2(l, m, n), \quad (3.13)$$

vii) Absorption and stimulated emission of 10.6 μm radiation by CO_2 ,

$$CO_2(100) + 2 \text{ photons (10.6 μm)} \leftrightarrow CO_2(001) + \text{photon (10.6 μm)}. \quad (3.14)$$

These energy-transfer processes are illustrated schematically in ***Fig. 3.3***, which also shows the energy levels of some of the CO_2 and N_2 vibrational states.

Equations (3.8) and (3.12) state that CO_2 molecule can be not excited only by collisions with excited N_2 molecules but also by electron and other particles collision. But by excitation mechanism of equation (3.12) a laser radiation cannot be obtained as seen from ***Fig. 3.3***. From excitation of CO_2 by electron bombardment lasing action can be obtained but as seen in ***Fig. 2.2*** excitation of CO_2 alone is not efficient as it is when excited with N_2-He gas mixture. Equation (3.14) is the process equation of lasing in CO_2-N_2-He gas mixtures. From this equation light amplification is clearly seen. When a 10.6 μm photon collides with a CO_2 molecule in (001) state two photons of the same wavelength are obtained.

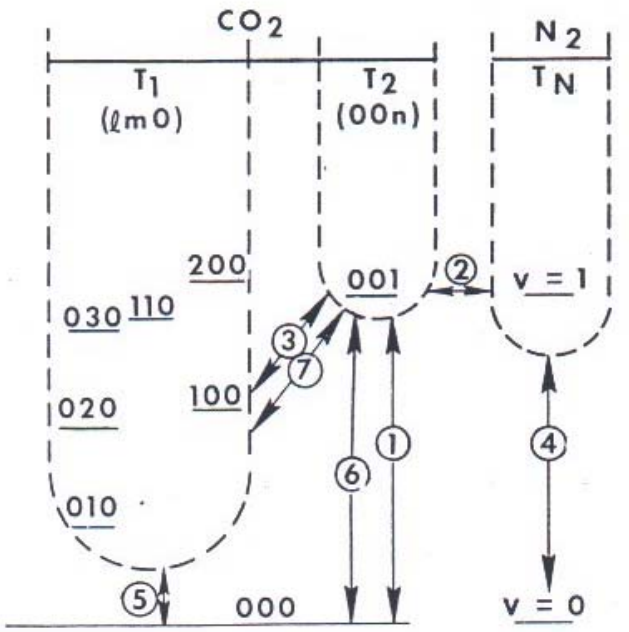

Figure 3.3- Diagram of some of the CO_2 and N_2 vibrational levels involved in the analysis.

CHAPTER 4

LASER BEAMS AND THEIR PROPERTIES

4.1- Transverse Modes of Laser Resonators

4.1.1- Intensity Distribution of Transverse Modes

In optical resonator electromagnetic fields can exist whose distribution of amplitudes and phases reproduce themselves upon repeated reflections between the mirrors. These particular field configurations compromise the transverse electromagnetic modes of a passive resonator.

Transverse modes are defined by the designation TEM_{mn} for Cartesian coordinates. The integers *m* and *n* represent the number of nodes or zeros of intensity transverse to the beam axis in the vertical and horizontal directions. In cylindrical coordinates the modes labeled TEM_{pl} and are characterized by the number of radial nodes *p* and angular nodes *l*. The higher the values of m, n, p, l, the higher the mode order. The lowest-order mode is TEM_{00} mode, which has a Gaussian-like intensity profile with its maximum on the beam axis. For modes with subscripts of 1 or more , intensity maxima occur that are off-axis in a symmetrical pattern. To determine the location and amplitudes of the peaks and nodes of the oscillation modes, it is

necessary to employ higher-order equations, which either involve Hermite or Laguerre polynomials. The Hermite polynomials are used when working with rectangular coordinates, while Laguerre polynomials are more convenient when working with cylindrical coordinates.

In cylindrical coordinates, the radial intensity distribution of allowable circular symmetric TEM_{pl} modes is given by the expression

$$I_{pl}(r,\phi,z) = I_0 \rho_l \left[L_p{}^l \rho \right]^2 \left(\cos^2 l\phi \right) \exp(-\rho) \tag{4.1}$$

with $\rho = 2r^2(z)/w^2(z)$, where z is the propagation direction of the beam, and r, ϕ are the polar coordinates in a plane transverse to the beam direction. The radial intensity distribution are normalized to the spot size of a Gaussian profile; that is *w(z)* is the spot size of the Gaussian beam, defined as the radius at which the intensity of the TEM_{00} mode is $1/e^2$ of its peak value on the axis. L_p is the generalized Laguerre polynomial of order *p* and index *l*. ***Fig. 4.1*** shows a 3D view of some of the TEM_{pl} modes.

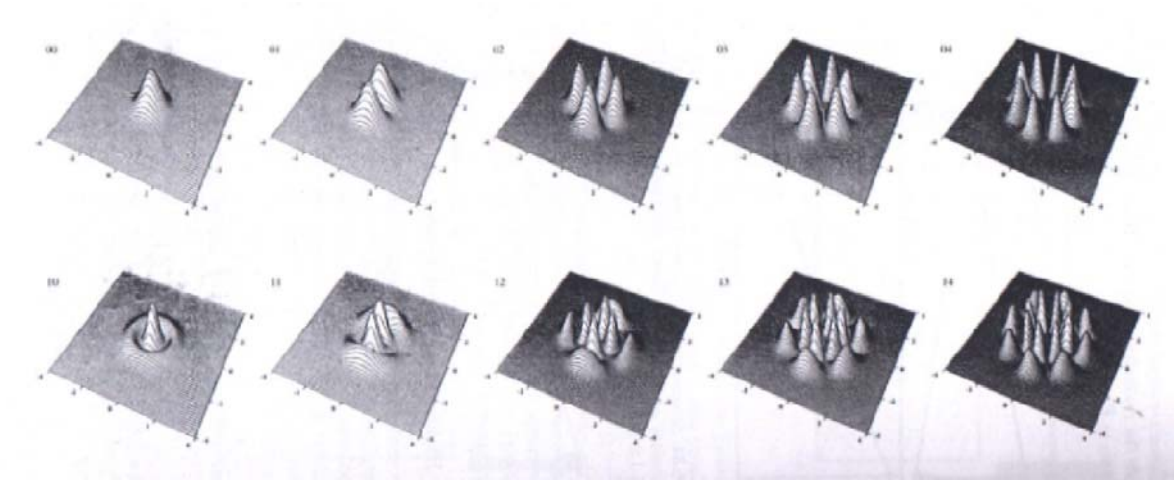

Figure 4.1- Intensity profile of higher transversal modes of stable laser resonators with circular symmetry [20]

4.1.2- Characteristics of Gaussian Beam

A light beam emitted from a laser with a Gaussian intensity profile is called the "Fundamental mode" or TEM_{00} mode. As a Gaussian beam propagates, its intensity distribution is Gaussian in every beam cross-section but the width of the intensity profile changes along the axis. The Gaussian beam contracts to a minimum diameter $2w_0$ at the beam waist where the phase front is planar. If one measures z from this waist, the expansion laws for the beam assume a simple form. The spot size, a distance z from the beam waist expands as a hyperbola, which has the form

$$w(z) = w_0 \left[1 + \left(\frac{\lambda z}{\pi w_0^{\,2}} \right)^2 \right]^{1/2} . \tag{4.2}$$

Its asymptote is inclined at an angle θ/2 with the axis, as shown in ***Fig. 4.2***, and defines the far-field divergence angle of the emerging beam. The full divergence angle for the fundamental mode is given by

$$\theta = \lim_{z \to \infty} \frac{2w(z)}{z} = \frac{2\lambda}{\pi w_0} . \tag{4.3}$$

From these considerations it follows that at large distances, the spot size increases linearly with *z*, and the beam diverges at a constant cone angle θ. From equation (4.3) it is clearly seen that the beams with larger diameters have smaller divergence.

At sufficiently large distances from the beam waist the wave has a spherical wavefront appearing to emanate from a point on the axis at the waist. If R(z) is the radius of curvature of the wavefront that intersects the axis at z, then

$$R(z) = z \left[1 + \left(\frac{\pi w_0^{\,2}}{\lambda z} \right)^2 \right] . \tag{4.4}$$

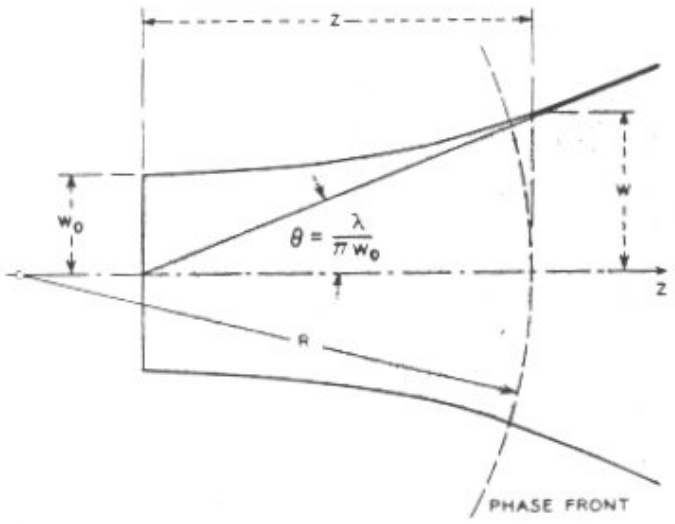

Figure 4. 2- Contour of a Gaussian beam

Also the wavefront of a Gaussian beam has the same phase across its entire surface. Sometimes the properties of a TEM_{00} mode beam are described by specifying a confocal parameter

$$b = \frac{2\pi w_o}{\lambda} \quad , \tag{4.5}$$

where b is the distance between the points at each side of the beam waist for which $w(z)=(2)^{1/2} w_o$.

4.1.3- Laser Resonator

Mode structure of a laser beam is directly related with the resonator configuration. Mode parameters of a resonator with unequal curvature mirrors are derived by Kogelnik and Li [21]. The geometry of such a resonator, where the radii of curvature of the mirrors are R_1 and R_2, is shown in ***Fig. 4.3***.

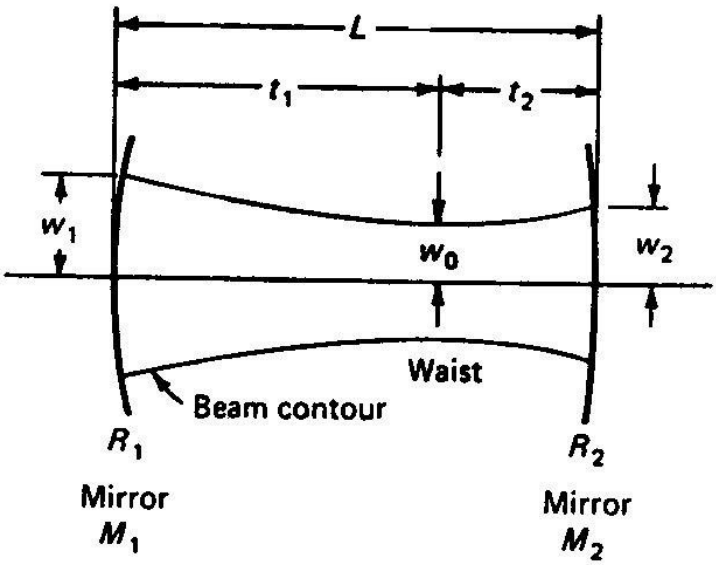

Figure 4.3 - Mode parameters of interest for a resonator with mirrors of unequal curvature

The diameters of the beam at the mirrors of a stable resonator, $2w_1$ and $2w_2$, are given by

$$w_1^4 = \left(\frac{\lambda R_1}{\pi}\right)^2 \frac{R_2 - L}{R_1 - L} \frac{L}{R_1 + R_2 - L} \tag{4.6}$$

$$w_2^4 = \left(\frac{\lambda R_2}{\pi}\right)^2 \frac{R_1 - L}{R_2 - L} \frac{L}{R_1 + R_2 - L} \quad . \tag{4.7}$$

The diameter of the beam waist $2w_o$, which is formed either inside or outside the resonator, is given by

$$w_0^4 = \left(\frac{\lambda}{\pi}\right)^2 \frac{L(R_1 - L)(R_2 - L)(R_1 + R_2 - L)}{(R_1 + R_2 - 2L)^2}. \tag{4.8}$$

The distances t_1 and t_2 between the waist and the mirrors, measured positive as shown in ***Fig. 4.3***, are

$$t_1 = \frac{L(R_2 - L)}{R_1 + R_2 - 2L} \tag{4.9}$$

$$t_2 = \frac{L(R_1 - L)}{R_1 + R_2 - 2L} \quad . \tag{4.10}$$

These equations treat the most general case of a resonator but they can be simplified for most of resonator configurations.

4.1.4- Stability of a Resonator

Resonators with regard to their stability are classified as stable and unstable resonators. In stable resonators rays are continuously refocused and ray content of the resonator is constant. However, in unstable resonators rays become more and more dispersed and they escape out of the resonator. But the “stability” referred to in

these resonator classifications is that of geometrical ray bouncing forth and back in the cavity designs mentioned above, and has nothing related with the stability and instability of laser oscillation in transverse modes.

Stability condition for a stable resonator is given as follows

$$0 < \left(1 - \frac{L}{R_1}\right)\left(1 - \frac{L}{R_2}\right) < 1 \quad . \tag{4.11}$$

This condition is derived from a paraxial ray tracing in a periodic convergent lens sequence. This periodic lens sequence is dual to spherical-mirror resonator.

To show graphically which type of resonator is stable and which is unstable, it is useful to plot a stability diagram on which each resonator type is represented by a point. This is shown in ***Fig. 4.4*** where the parameters L/R_1 and L/R_2 are drawn as the coordinate axes; unstable systems are represented by points in the shaded areas.

Various resonators types, as characterized by the relative positions of the centers of curvature of the mirrors, are indicated in the appropriate regions of the diagram. Also parameters g_1 and g_2 are shown in the figure.

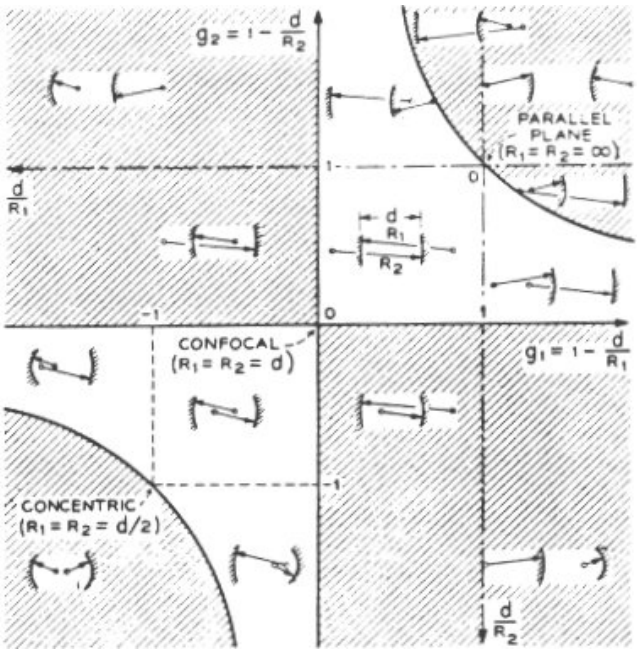

Figure 4. 4- Stability diagram. Unstable resonator systems lie in the shaded region[21]

4.2- Beam Propagation Factor

For applications of laser beams the characterization of their transversal mode structure is necessary. Both the beam diameter at the waist $2w_o$ and the beam divergence θ has to be determined for this purpose. The quality of laser beams can be described by the beam parameter product BP:

$$BP = \theta \, \omega_o \tag{4.12}$$

BP is minimum for diffraction-limited beams.

The values of θ and w_o have to be obtained experimentally. One simple method is the measurement of the spot size diameter d_{focus} of the beam at the focal length of a lens as shown in ***Fig. 4.5***.

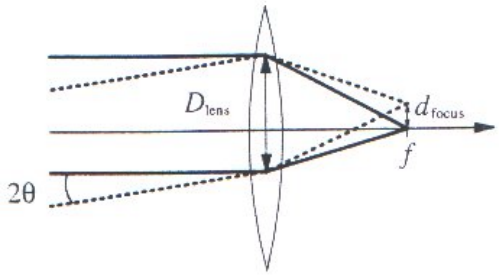

Figure 4.5- Divergence determined by measuring the waist size behind a focusing lens

The divergence angle can be determined from the focal length f and the diameter d_{focus} in the focal distance of the lens by:

$$\theta = \frac{d_{focus}}{2f} \ . \tag{4.13}$$

The beam parameter product can be calculated from

$$BP = \frac{D_{lens}.d_{focus}}{4f} \tag{4.14}$$

with the beam diameter D_{lens} at the position of the lens and the focal length f.

The quality of a measured beam is described by the ratio of the beam parameter products of this beam BP_{beam} relative to the best possible value BP_{Gauss} of a Gaussian beam of the same wavelength λ in the same material with refractive index n. This ratio is defined as beam quality or beam propagation factor M^2 :

$$M^2 = \frac{BP_{beam}}{BP_{Gauss}} = (\theta\, \omega_{waist})\frac{\pi n}{\lambda}. \tag{4.15}$$

Thus M^2=1.5 means the beam parameter is 1.5 times worse than the best possible value for the wavelength and thus the focus for a given lens would show 1.5 times larger diameter as for a perfect beam.

4.3- Focusing of a Laser Beam

Focusing a laser beam is of great importance in material processing. Positioning of a beam in specified location with specified spot size is the main purpose of focusing. In all focusing methods the laws of geometric optics are sufficient but to calculate the precise spot size and focal depth one needs to refer to Gaussian optics and diffraction theory.

4.3.1- Diffraction Limited Spot Size

A beam of finite diameter is focused by a lens onto a plane as shown in ***Fig. 4.6***. The individual parts of the beam striking the lens can be imagined to be point radiators of a new wave front. The lens will draw the rays together at the focal plane and thus constructive and destructive interference will take place. There will be observed a Fraunhofer Diffraction Pattern. The central maximum will contain approximately 86% of all the power in the beam. The diameter of this central maximum will be the focused beam diameter, usually measured between the points where the intensity has fallen to $1/e^2$ of the central value.

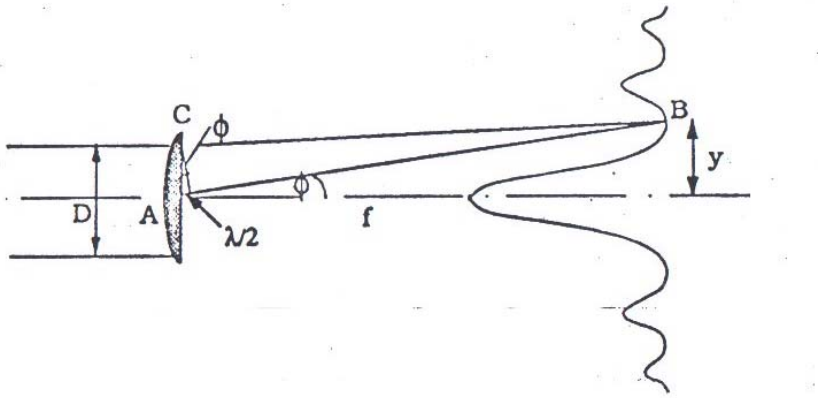

Figure 4. 6- Diagram illustrating the diffraction limited spot size

Equation for the spot diameter of the fundamental mode of a circular beam is given by

$$d_{\min} = 2.44 \cdot \frac{f\lambda}{D} \tag{4.16}$$

where D is the beam diameter on the lens and f is the focal length of the lens. The diameter of diffraction limited spots for other modes (TEM $_{pl}$) of a laser beam is given by

$$d_{\min} = 2.44 \cdot \left(\frac{f \cdot \lambda}{D} \right) (2p + l + 1). \tag{4.17}$$

4.3.2- Effects of M^2 on Focusing

Beam quality is a property of a beam and should have influence on the beam size obtained after focusing. In focusing of Gaussian beam the diffraction limited Gaussian spot size is:

$$d_{\min} = \frac{4f\lambda}{\pi D}. \tag{4.18}$$

But not every beam is Gaussian so a correction by M^2 should be applied. As it was previously mentioned that the spot size of a focused beam is M^2 times that for a perfect beam. So the equation is given by

$$d_{\min} = \frac{4f\lambda}{\pi D} \cdot M^2. \tag{4.19}$$

4.3.4- Spherical Aberration

There are two reasons why a lens will not focus to a theoretical point; one is the diffraction-limited problem discussed above and the other is that a spherical lens is not a perfect shape. Most lenses are made with a spherical shape since this can be accurately manufactured without too much cost and the alignment of the beam is not so critical as with a perfect aspheric shape. The net result is that the outer ray entering the lens is brought to a shorter axial focal point than the rays nearer the center of the lens, as shown in ***Fig. 4.7***. This leaves a blur in the focal point location. The plane of best geometric focus (the minimum spot size) is a little short of the plane of the plane wavefront, the paraxial point.

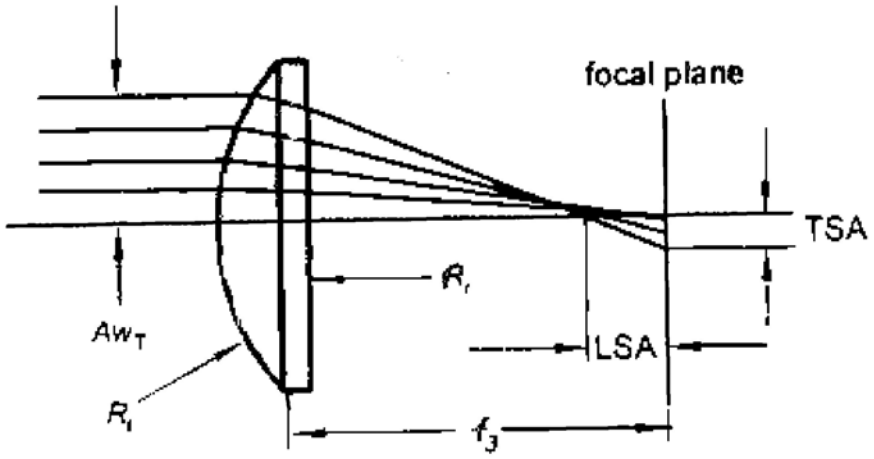

Figure 4.7- Spherical aberration of a single lens focusing a parallel beam

Focusing of a collimated beam produces a transverse spherical aberration (TSA) and a longitudinal spherical aberration (LSA) shifts as shown in ***Fig. 4.7***. To a first approximation the focus diameter of the part due to the aberration of lens f_3:

$$d_a = K(n,q)\frac{D^3}{f_3{}^2} \quad , \tag{4.20}$$

where

$$K(n,q) = \frac{1}{32}\frac{1}{n(n-1)}\left[\frac{(n+2)}{(n-1)}q^2 - 4(n+1)q + (3n+2)(n-1) + \frac{n^3}{n-1}\right] \tag{4.21}$$

with

$$q = \frac{R_2 - R_1}{R_2 + R_1} \tag{4.22}$$

R_1- lens entrance radius

R_2- lens exit radius

n- lens refractive index.

In spherical aberration shape parameter q determines the degree of the aberration. ***Fig. 4.8*** shows the axial difference in focal length (LSA) with respect to parameter q. Here the focus length for different shapes is constant. Here it is clearly seen that spherical aberration decreases for a plano-convex lens mounted in one way than the other.

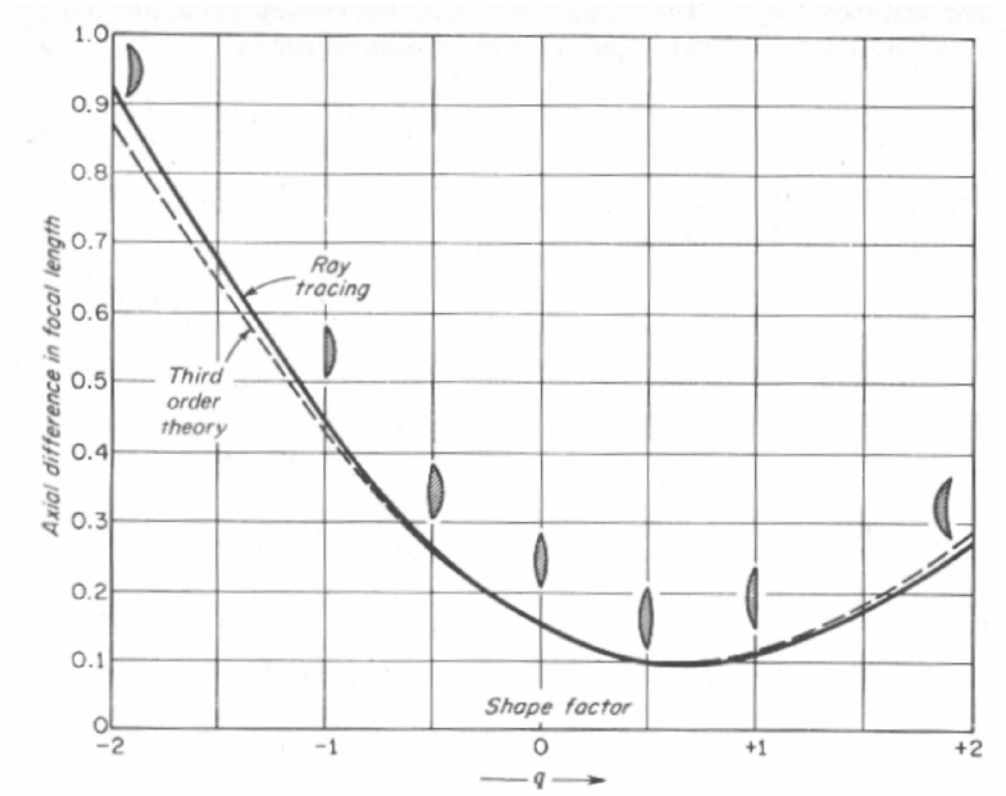

Figure 4.8 - A graph of spherical aberration for lenses of different shape but the same focal length [22]

4.3.5- Depth of Focus

The depth of focus is the distance over which the focused beam has approximately the same intensity. It is defined as the distance over which the focal spot size changes by ± 5%. It is given by

$$z_f = \pm\pi\sqrt{\left(\rho^2 - 1\right)}\frac{r_o^{\,2}}{(2p + l + 1)\lambda}, \tag{4.23}$$

where ρ is the fractional incrase in beam diameter and *p,l* show the TEM supscripts.

CHAPTER 5

DESIGN OF SLOW AXIAL FLOW CO_2 LASER

A laser is designed for use in a specified application, so design parameters should be defined accordingly. Starting with the application needs one should derive the properties of the resonator. In ***Fig. 4.3*** the basic resonator specifications, resonator length, place of waist, spot sizes on mirrors etc., are shown and these should be determined. Calculations are given in Appendix I.

5.1- Laser Applications and Specification of Laser Output Beam Parameters

Applications that are considered to be done in this thesis work are cutting and welding of metals, polymers and ceramics. For applications related to cutting it is desirable to have a laser with TEM_{00} mode of operation. Transverse electromagnetic mode of operation of lasers used in welding applications is usually $TEM_{00} + TEM_{01}^{*}$. Also it is good to have a beam with small angle of divergence in order of mrad's. Desired cutting thickness for ordinary carbon steel is 2 mm, and for welding it is 0.5 mm. Power needed for such applications is around 200 Watts of 10.6 μm laser

radiation. As a result of these application needs the laser should have the following output beam and power properties:

- Laser Power : 200 W
- Beam Mode : TEM_{00} +TEM_{01}*
- Beam Divergence: mrad.

5.2- Determination of Laser Resonator Parameters

Starting with the application needs parameters, resonator type, resonator length, tube bore diameter, size and types of mirrors used, transmission of output coupler is the most important parameters to be determined.

5.2.1- Resonator Type

Some possible resonator configurations are given in ***Fig. 2.12***. For the design hemispherical resonator configuration is selected. This type of resonator has one plain output coupler and a spherical end mirror. The advantage of this type is to know exactly the place of the beam waist. Place of the waist and its size are the key parameters that are needed to estimate beam diameter a distance far away from the resonator. This also helps to calculate the spot size of the focused beam.

To save space it is decided to have U-bend resonator. By using such a resonator without changing the discharge length overall length of the laser is lowered to half of the resonator length. Also having such a resonator guarantees to have a laser beam with linear polarization [26].

5.2.2- Discharge and Resonator Lengths

As a general rule lasers operated in slow flow regime have output powers of 50 W/m for TEM_{00} and 75 W/m for TEM_{00}+TEM_{01}* mode of operation. In length calculations 75 W/m value will be considered since radiation of the fundamental mode is also present there. For power of 225 Watts we should have a discharge length of 3 m. For usual resonators, resonator length is about 25% larger from the discharge length and resonator length of 3.75m is obtained for the design. Mirrors of the resonator should be as far as possible from the electrodes to avoid any contamination from sputtering of electrodes, electrode material vapor deposition and from any gas impurities.

5.2.3- Determination of End Mirror Curvature and Stability Check

To determine the curvature of the end mirror first of all the beam divergence should be exactly specified. Then by using equation (4.3) beam waist w_o (radius of the beam on output coupler) should be calculated. Inserting that value in equation (4.8) radius of curvature of the end mirror R_2 can be calculated.

In this work a mirror with R_2=8 m was used. Radius of the beam waist was calculated as w_o= 3.67mm and divergence for the fundamental mode was calculated as 1.839 mrad. This value of divergence is sufficient for the thesis applications but can be lowered by changing the curvature of the end mirror.

Having determined both mirror curvatures, stability of the resonator should be checked by using inequality (4.11). Product g_1g_2=0.531 and resonator is in the stable region.

5.2.4- Determination of Laser Tube Bore Diameter

Having in hand values for $R_1 = \infty$ and $R_2 = 8$ m it is possible to calculate the beam spot size on both mirrors. Since it was previously specified that the laser will operate to its TEM_{01}* mode, in determination of tube bore diameter, spot size of the second mode should be used. In calculation of beam diameters on the mirrors equations (4.6) and (4.7) will be used. Beam diameter on the output coupler is small than the beam diameter on the end mirror and for that reason in determination of tube bore diameter only the beam spot size on the end mirror will be considered. Beam diameter on the end mirror for the second mode is 15.1 mm and the bore diameter was selected to be 16.4 mm, which is the closest to our calculated value in the market. Also the beam on the output mirror will have a diameter of 11 mm.

5.2.5 – Determination of Output Coupler Transmittance

Most important parameter that should be determined in design of laser is the transmittance of output coupler. To determine this parameter equation (2.2) should be used. By plotting efficiency versus transmittance curve, the transmittance giving maximum efficiency is the optimum transmittance of the output coupler. To plot this curve we need the reflection of end mirror, cavity losses and small signal gain of the active medium.

Cavity losses are generally the absorptions of total reflector mirrors used in the cavity and diffraction losses due to diameter changes inside the cavity along the beam path. Losses of cavity are increasing during the life period of resonator mainly due to contaminations on the cavity mirrors. These contaminations arise from vapor of electrodes used, sputtering and dust contained in gas mixture. Because of that increase in cavity losses, efficiency curves are plot for different loss factors.

Small signal gain and saturation intensity characterize the discharge medium

and should be used in every calculation related with the output parameters of the resonator. Since from Rigrod's equation saturation intensity is canceled to give efficiency of coupling there is no need to have that parameter. But in any case small signal gain should be known. This parameter can be determined experimentally. Also there are computational methods to derive this parameter but these methods are not in the scope of this study. To specify this parameter we should refer to previously done experimental works. Using ***Fig. 2.5*** small signal gain of 0.5 %/cm was obtained and used in calculations.

Plot of efficiency versus transmittance curve is given in ***Fig. 5.1***. In plot, curves for different loss values are given and transmittance of 20% for the output coupler was selected.

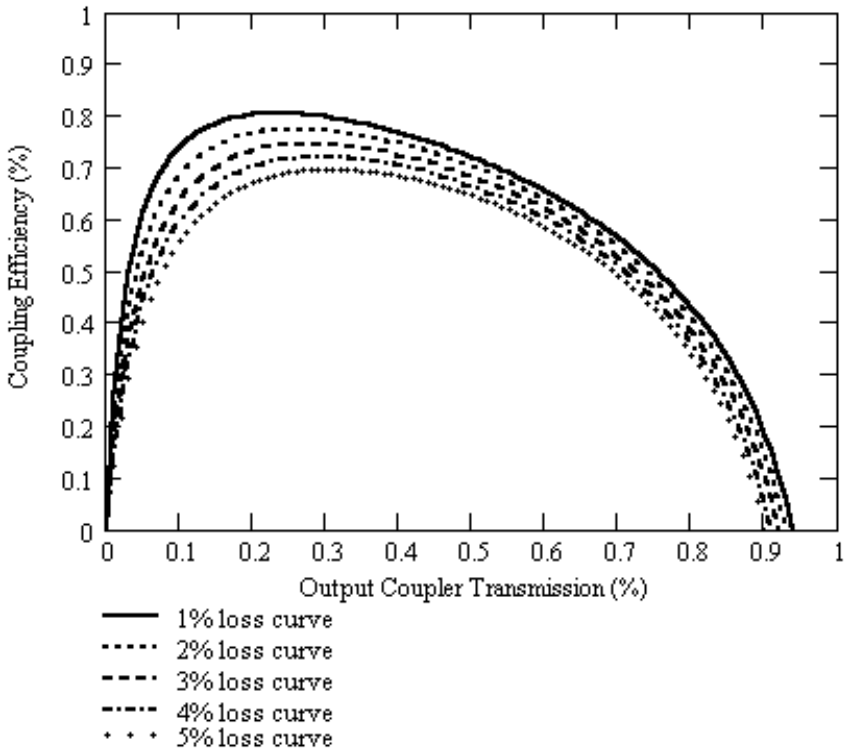

Figure 5.1 - Output coupling efficiency versus transmittance plot

5.2.6 – Selection of Mirror Material

In previous section it was stated that in time of operation contamination of optics surfaces increases and that increase causes absorption of radiation which results in increase in optics temperature. Temperature increase results in thermal expansion, which causes change in refractive index of material. Output coupler subjected to temperature change behaves like a lens (diverging or converging), changing the properties of output beam. For curved total or partial reflectors increase in temperature results in dimension changes from which curvature change is the most critical one. Change in curvature causes change in the previously predicted beam properties. Also since the radiation possesses Gaussian intensity profile and not all the surface is irradiated, curvature change is different for any point on a particular surface.

As a result, in selection of mirror materials thermal and optical properties of different materials used in CO_2 laser resonators will be studied. A formula including thermal expansion coefficient, thermal conductivity, refractive index gradient and percentage absorption for particular material will be used to obtain relative figures of merit. Formulas [28] are:

$$F = \frac{K}{AX_{1,2}} \tag{4.1}$$

where

K: thermal conductivity

A: total absorption

$X_1 = \frac{dL}{dT} + \frac{dn}{dT}$: thermal expansion coefficient plus refractive index gradient

or

$X_2 = \frac{dL}{dT}$: thermal gradient.

X_1 is used for lenses, windows and output couplers where effects of both focusing and surface distortion are important. X_2 is used for total reflectors where effect of only surface distortion is important. Also X_2 is used for output couplers when the effects of focusing can be ignored.

Material properties of materials studied are given in Appendix I. Plots for figure of merit versus absorption are given below.

5.2.6.1- Material selection for Output coupler

Output coupler material was selected between four materials: GaAs, Ge, KCl and ZnSe. Plots for the two cases: (1) focusing and surface distortion and (2) surface distortion only were examined.

From the plots of ***Fig. 5.2*** it is observed that KCl is best when focusing is of great importance, which is for high power lasers, but when surface distortion only is a concern performance of KCl is worst among the others. KCl is very good for high power lasers but needs extra conditioning facilities since it is hydroscopic in nature and for low power laser where focusing is not problem its performance is worst so it is not applicable in our design.

GaAs is best when only surface distortion is considered and performs close to ZnSe and Ge when both focusing and surface distortions are important. GaAs cannot be easily found in the market and also it is not transparent in visible region (transparency in visible region is advantage in alignment facilities) so it also is not applicable.

Ge, in performance sequence comes after GaAs but thermal runaway is near 100 ^{o}C and is not applicable to our design.

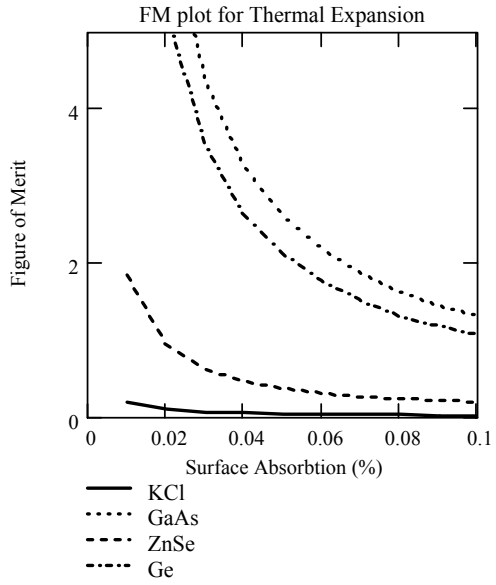

a) for X= X_2

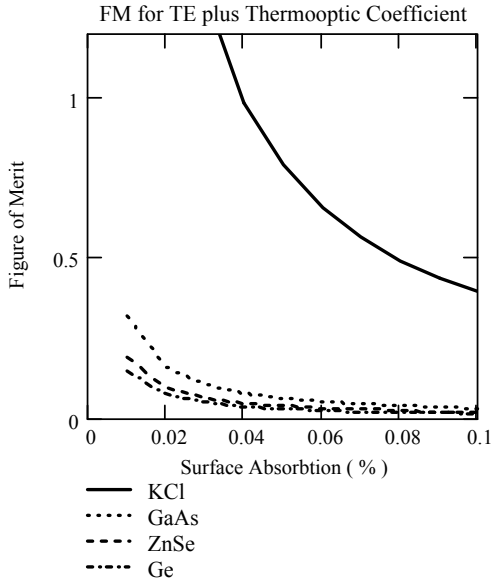

(b) for X=X_1

Figure 5.2 - Optical distortion figures of merit compare substrate materials for CO_2 laser output coupler

ZnSe is average in performance but runaway temperature is about 300 ^{o}C, can be easily found in the market, and is transparent in visible region. Also it is cheap in comparison to Ge and GaAs. As a result ZnSe is selected as material for the output coupler.

5.2.6.2- Material selection for full reflector mirrors

Full reflector mirrors substrate material was selected between four materials: Cu, Mo, Si and Ge. Only the case of surface distortion was examined.

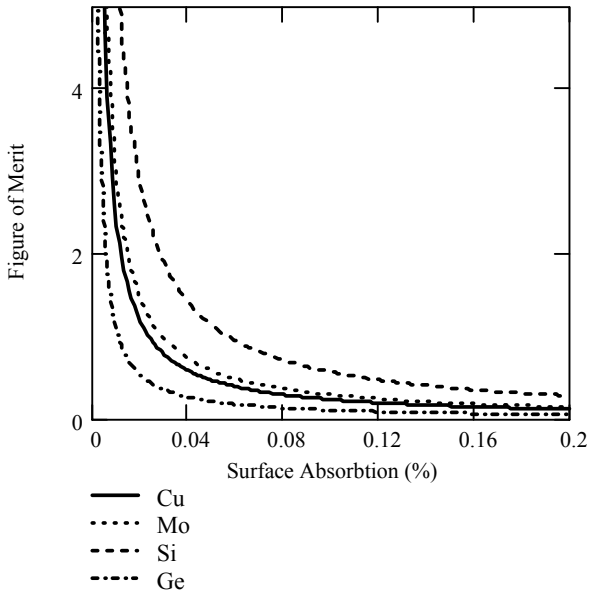

Figure 5.3 - Optical distortion figures of merit compare substrate materials for CO_2 laser full reflector mirrors

From the plot in ***Fig. 5.3*** it is seen that silicon substrates perform best but performance of coatings on silicon is less from that on copper. Molybdenum is second in performance and is widely used in not very clean operating conditions. Germanium having a very low runaway temperature is not good for lasers with high power. Copper on the other hand is in third position but metallic coatings perform best on it. Cooling of copper is very easy compared to other materials. For the design copper substrate mirrors were selected, end mirror with 99% reflection and bending mirrors with 99.9 % reflection were selected.

CHAPTER 6

EXPERIMENTS CARRIED OUT ON THE DESIGNED LASER

6.1- Experiments on Laser Gas and Electrical Feeding

In the previous chapter laser design parameters were determined and considering these parameters a resonator was designed and constructed. Technical drawings and a picture of the final construction of resonator are given in Appendix II. In this part laser output beam characteristics, input power, current, gas pressure and gas composition will be measured and relations between these parameters will be determined.

6.1.1- Laser System Set up

Designed laser is driven by 25 kV power supply which delivers 50 mA current. Voltmeter shown in ***Fig. 6.1*** directly measures the voltage on the capacitor of supply. Ammeter is connected to the supply end and total current delivered to

the system is measured. SCR`s group is consisted of trystors and resistors which ensure the ignition of both tubes at the same time. Also resistor R_2 is a part of the ignition system. Resistors R_1 are the ballast resistors which sustain current delivery to the discharge after ignition.

Gas mixture of CO_2:N_2: He is delivered to the system by three tubes which separately contain the three gases. Mixture composition is arranged by flow meters connected to each tube. Gas inlet is at the anode side of the resonator. Exhaust gas is pumped out by vacuum pump and the pressure inside the resonator is measured by a vacuum gage.

Laser radiation is measured by a power meter having a range of 0-250 W for CO_2 lasers.

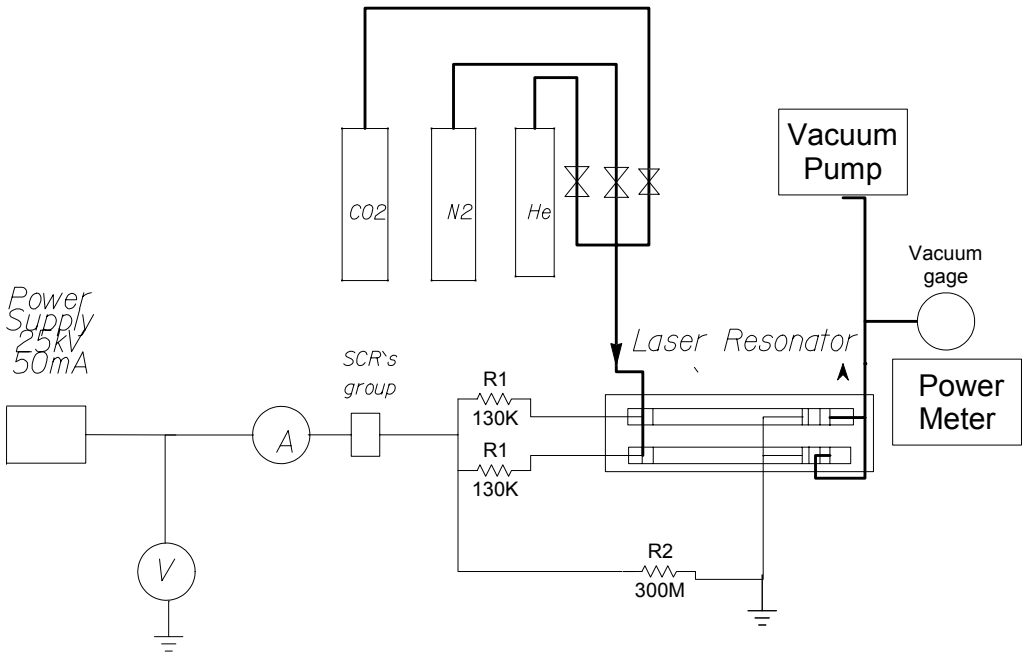

Figure 6.1- Experimental setup

6.1.2- Current - Partial Pressure Characteristics of Laser Discharge

Having three different gases, keeping the pressure and flow rate of two of them constant and changing the pressure of the third gas the behavior of individual gases in the discharge is obtained. Current-Partial pressure characteristics were obtained by maximizing the output power of the laser and at that instance current, operating potential and total gas pressure were recorded. The plots of current versus partial pressure of one constituent of the mixture are given in ***Fig. 6.2***.

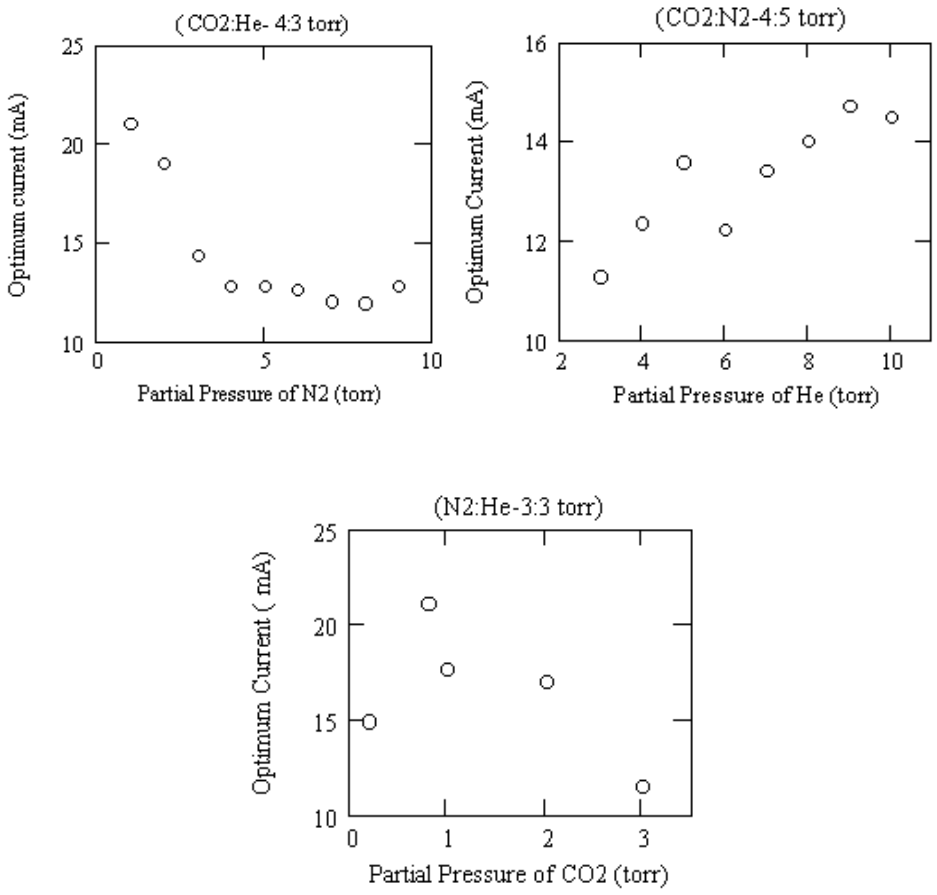

Figure 6.2 - Current -Partial Pressure behavior of laser gas constituents

Each gas has different effect on the optimum current that gives maximum power. Keeping constant pressures of CO_2 and He, current decreases with increasing partial pressure of N_2. Also keeping constant pressures of N_2 and He and increasing the pressure of CO_2 current behavior is similar to N_2 gas instead of that when partial pressure of CO_2 is less than the partial pressure N_2 current is increasing. But current characteristics of He is completely different from the other two constituents, increasing the partial pressure of He allows the increase of current to obtain maximum output laser power.

6.1.3- Effects Partial Gas Pressures on Output Laser Power

Keeping constant pressure of the other two gases and changing the pressure of the third gas output power was measured for the three gases. ***Fig. 6.3*** gives the measured results of partial gas pressure and corresponding output power for optimum current. As it is clear from the figures below CO_2 and N_2 have similar effects, both increase the output power to some maximum value and then with increase of their partial pressure output power decreases. In contrast to CO_2 and N_2 partial pressure effects, increase in partial pressure of He results in increase in output laser power. During the experiments saturation for He pressure was not found since the power delivered from the supply has reached its limit but it can be observed from the ***Fig. 6.3*** that rate of power increase decreases with the increase of partial pressure of He.

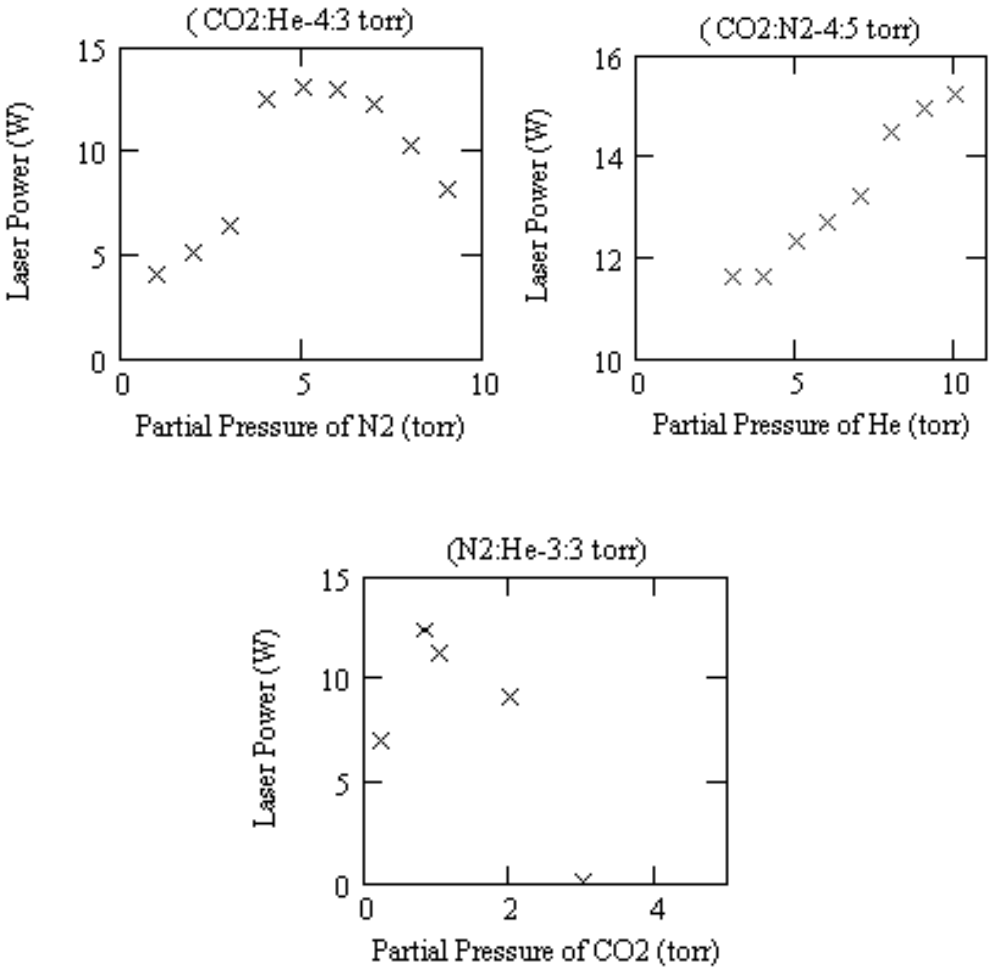

Figure 6.3 - Effect of Partial pressures on output power

6.1.4- Effects of Gas Composition on Output Power

It should be also noted that the output power strongly depends on gas composition. So it is of great importance to study the composition rates of all the three gases at the same time. To make such comparison partial pressures of individual gases were divided by total pressure so that the sum of the ratios results in unity. Plotting contour graphs for two of the gas ratios and having as a third variable the output power the effects of the constituent gases on the output power is obtained.

From the plots the third gas ratio is found by subtracting the sum of the two gas ratios from one. Results are present in ***Fig. 6.4***.

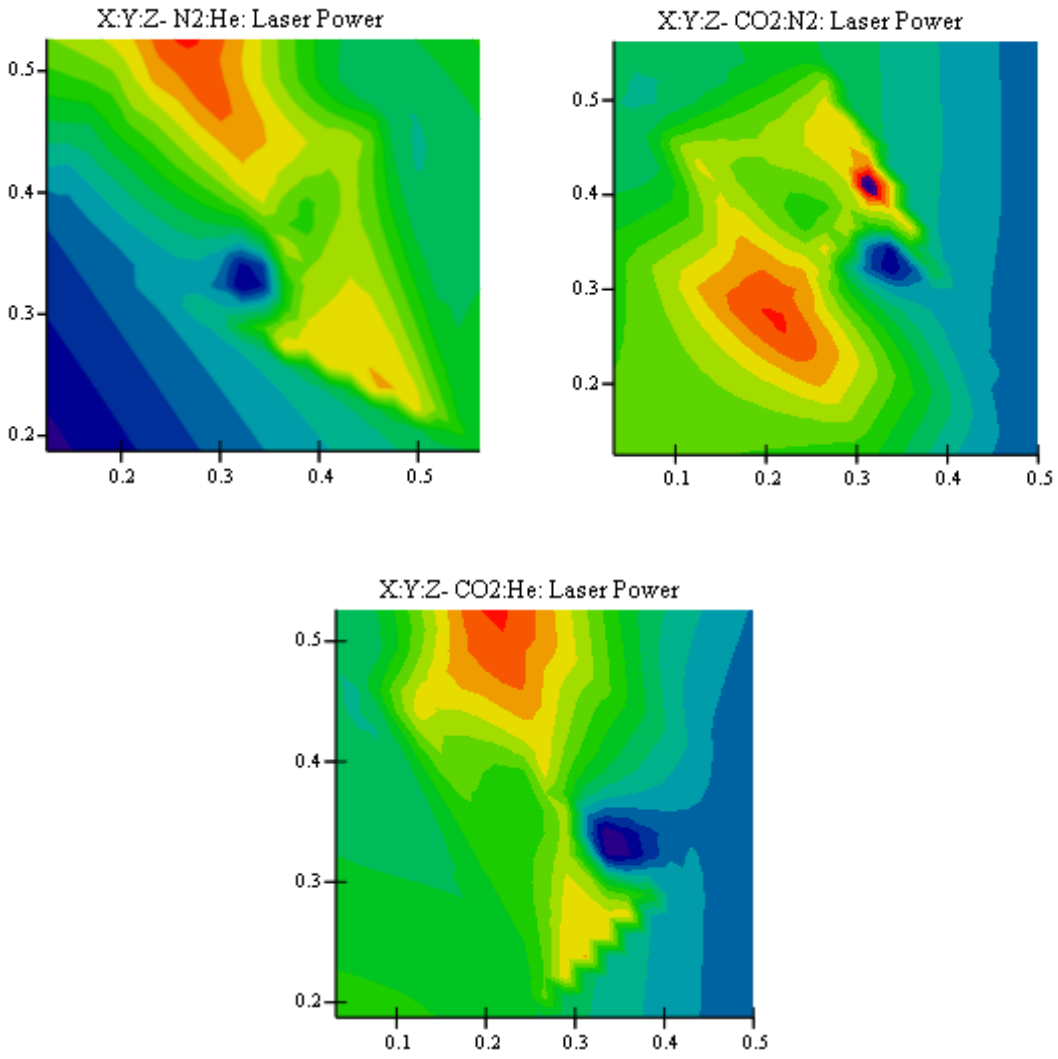

Figure 6.4 - Gas composition effects on Output Power

From the results illustrated in *Fig. 6.4* we can conclude that the ratio between the composition rate of CO_2 and N_2 is 1to 1.5 respectively. Rate of He is very much

than the proportions of CO_2 or N_2. In gas content optimization it is more reasonable first to fix the values of CO_2 and N_2 and then to increase the content of He until maximum power is obtained.

6.1.5 – Laser Discharge with Constant Gas Composition

Up to now effects of individual laser gas constituents were studied and an optimum gas composition at partial pressure ratios of (CO_2:N_2:He-1:1:6) was selected. Total pressure was 23 torr and current was changed so that to obtain a graph indicating effects of power input in the discharge. As in previous experiments current, potential and output laser power were recorded.

Fig. 6.5 shows effect of increasing current on laser output power. As current increases laser power also increases up to a maximum power and starts to decrease with subsequent increase in current. Here the behavior of current is identical to the behavior of input power and the graph also indicates that much power does not mean much laser output power since the lasing medium is heated up and this decreases lasing effect of the discharge.

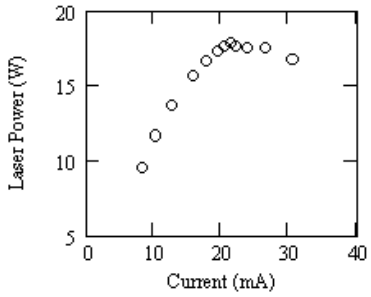

Figure 6.5- Effect of current on laser power

Fig. 6.6 depicts the effect of current on the electric to optical efficiency of the laser. Increase in current decreases the efficiency of the system and for efficient operation its better to have less current. Having less current means less input power but it does not mean maximum output laser power as can be observed from ***Fig. 6.7***. If ***Fig. 6.5*** and ***Fig. 6.7*** are examined at the same time it is clear that the plot in ***Fig. 6.7*** is the mirror image of the plot in ***Fig. 6.5***. This indicates that as the input power increases the conversion of electrical power to radiation power decreases. And this decrease in efficiency is related to the increase in temperature of the discharge and to the increase in power dissipation in the ballast resistors.

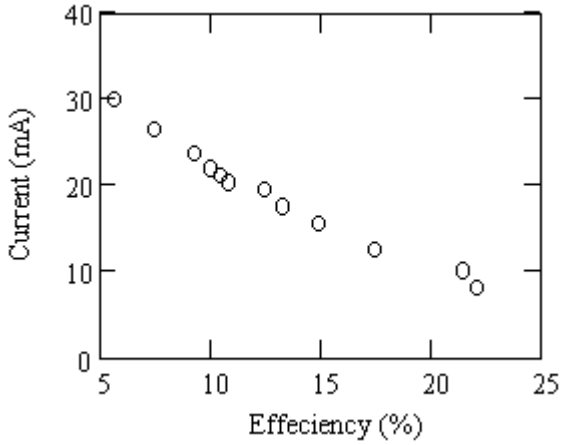

Figure 6.6 - Efficiency versus Current graph

To study the effects of pressure rise on output laser power a constant mixture of volumetric composition CO_2:N_2:He-8.9:13.4:77.7 was used. During the experiment flowing gas pressure, output laser power, potential and optimum current that maximizes the output power were recorded. Effects of input power and pressure on the output power are plotted in ***Fig. 6.8*** and ***Fig. 6.9*** respectively. According to ***Fig. 6.8*** laser power is directly proportional to input power but it saturates after some pressure limit. This implies that after some pressure limit it is not possible to increase

the laser power further. This result can be seen more clearly from the contour plot in ***Fig. 6.10***. In that figure red parts indicate the region of maximum laser power and it is reached for an input power of 140 W and total pressure of 100 torr. And any further increase in pressure or input power has very little effect on laser power.

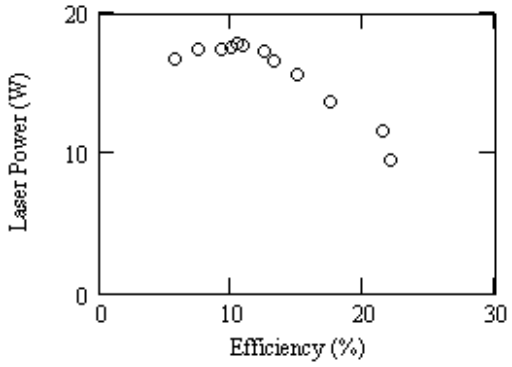

Figure 6.7 - Efficiency versus Laser Power graph

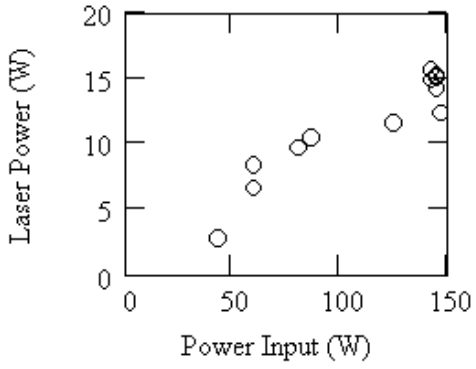

Figure 6.8 - Effects of Input Power on Output Laser Power

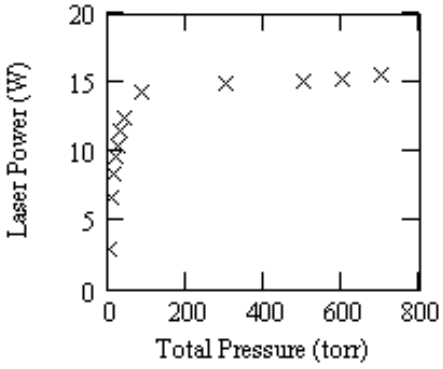

Figure 6.9 - Effects of Pressure on Output Laser Power

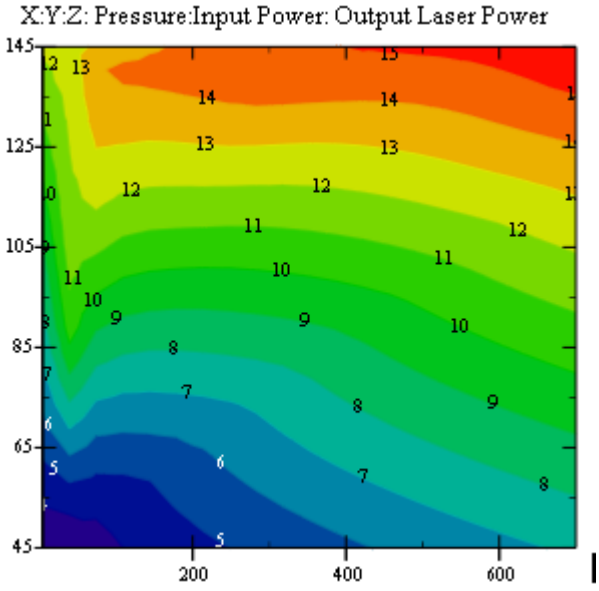

Figure 6.10 - Contour Plot of Combined effects of Pressure and Input Power on Output Laser Power

6.1.6- Maximum Power Obtained

During the experiments carried out above a general relation between the gas composition and electrical feeding of the system was investigated. So these results should be evaluated qualitatively since quantitative results do not reveal the maximum obtainable power of the design. Maximum power was obtained under pressure which was not detectable by our instruments but it was near the atmospheric pressure. That maximum power was also realized by the constant mixture of volumetric composition CO_2:N_2:He-8.9:13.4:77.7 and current of 20 mA. Power obtained was 32 W and a photo showing the power meter digital display is given in ***Fig. 6.11***.

Figure 6.11 - Maximum Power Obtained for Single Tube Operation

6.2- Experiments on Laser beam Properties

6.2.1- Laser Beam Profiling

Intensity distribution measurement on the cross section of a beam was performed. A pinhole with diameter much smaller than the beam diameter was moved in a plane cutting the beam perpendicular to its path of propagation. A pinhole of 0.8 mm in diameter was used to profile the intensity distribution of a beam with 9 mm in diameter. Also the pinhole plate was coated with graphite to prevent back reflections of radiation into the resonator. ***Fig. 6.12*** depicts the method of measurement. Circle with dashed lines shows the laser beam. Moving the pinhole in x and y-directions a two dimensional array of power data was obtained. Beam power passing through the pinhole was measured by a power meter placed behind the pinhole plate. Increments of displacement ΔX and ΔY in x and y-directions respectively were kept constant to eliminate additional data analysis. During the measurements after completing one row of power sampling the pinhole plate was removed and total power of the laser beam was checked to ensure that the beam power was constant in the period of sampling. Since the pinhole plate was moved by an X-Y stage there was no considerable errors in placing the pinhole at place where it was desired to be. It should be noted that the profile is also strongly dependent on optics alignment and to assure constant alignment mirror adjusting screws were kept at the same position during all measurements on beam profiling. Power changes were compensated by pressure adjustments and keeping the current of operation constant. To eliminate effects of composition changes in operating gas a constant mixture gas was used. The diffraction of the sample beam passing through the pinhole was not considered since the aim is not to obtain absolute powers but relative power distributions over the beam cross-section. This will not affect the beam profile results but a precaution was taken by placing the power meter just behind and very close to pinhole plate such that to absorb all the radiation passing the pinhole.

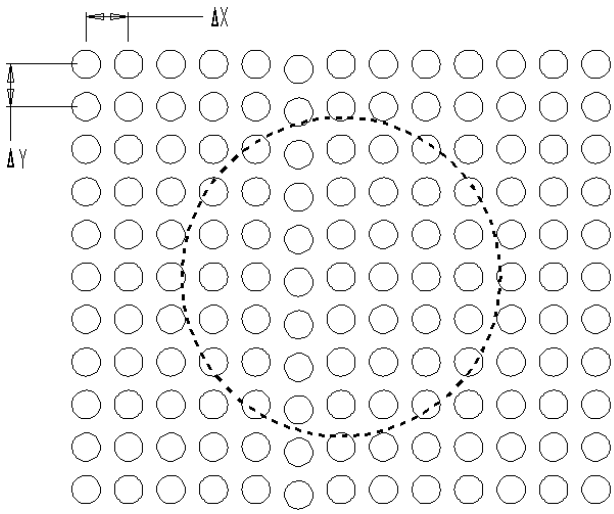

Figure 6.12 - Beam Profiling Method of Laser Beam

Obtained data were collected as square matrices and 3-D plots giving directly the beam intensity distribution were obtained. X and y-axes are the same as they were in measurements and the z-axis is the power, which are matrix elements. Plot of raw data does not look very nice and also it represents the values of the data points only and surrounding points remain under the lines joining data points. It is obvious that there is no any sharp edge in the intensity distribution of a beam as it is observed in the plot of raw data. To eliminate such results either a very small pinhole should be used or data analysis of the measurements should be done. Plot of raw data is given in Appendix III.

In data analysis instead of joining data points with lines a curve was fitted over all data points. Method used is known as cubic spline fitting and fits a third order polynomial to data. Such an analysis results in approximation of points which were not sampled and gives more realistic plots. In data analysis a package program MathCAD® was used and a sample calculation sheet is given in Appendix III for 10 Watt beam.

Beam profiling was done for three beams with different power so that it will be

possible to investigate the effects of beam power on the intensity distribution of the beam. ***Fig. 6.13*** gives the asymmetric and top vies of the 3-D plots for 10, 20 and 30 watt laser beams.

As it is observed from the plots in ***Fig. 6.13*** asymmetric views give the intensity profile of a beam but do not give clear information about the shape of the beam cross-section. To obtain beam cross-section shape a top view of the profiling plot is needed and this plot is given also in ***Fig. 6.13***. From the plots it is observed that the beam is more intense in its center and intensity decreases going away from the center. And also it is clear that the beam shape of the obtained laser beam is not an exact circle as it was desired to be obtained. The shape of the beam changes to elliptical one as the power of the beam increases. This change in beam shape can not be observed from beam burns obtained on wood (***Fig. 6.14***). Although burn patters look like a circle the intensity profiles of the beams show that they are not. This difference is mainly the result of thermal conductivity of material on which burns are obtained. May be with materials, having lower thermal conductivity and high absorption of the laser radiation, burns close in shape to the profiles could be obtained.

The change of beam profiles with increasing powers may be a result of increasing power in the discharge and increasing gas pressure. The increased discharge power has destructive effects on the distribution of small signal gain in the active medium and this will result in change in the beam profile. To eliminate such drawbacks of increased power, cooling rate of active medium should be increased either by decreasing the temperature of cooling water or increasing water flow rate or by increasing the gas flow rate. None of these methods were applicable during the experiments.

The effect of increased pressure on the beam profile is in connection with the change in alignment of cavity optics. Since the optics are placed on O-rings to ensure a good vacuum, easy replacement and easy cleaning there are finite movements in any pressure change. As a consequence of these finite displacements output power of the laser will not change by distinguishable amount but beam profile will change destructively.

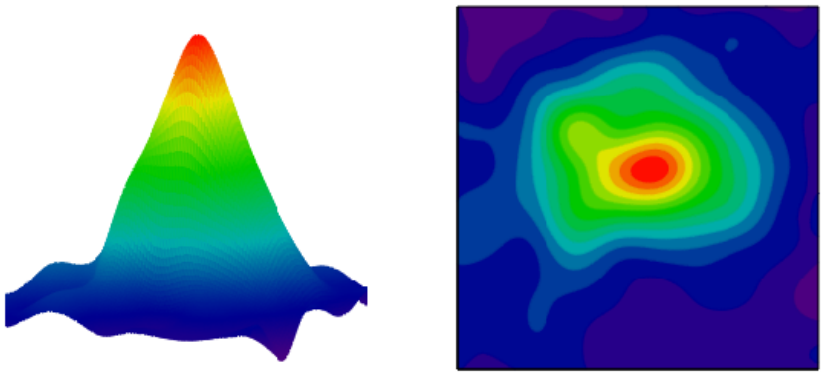

a)

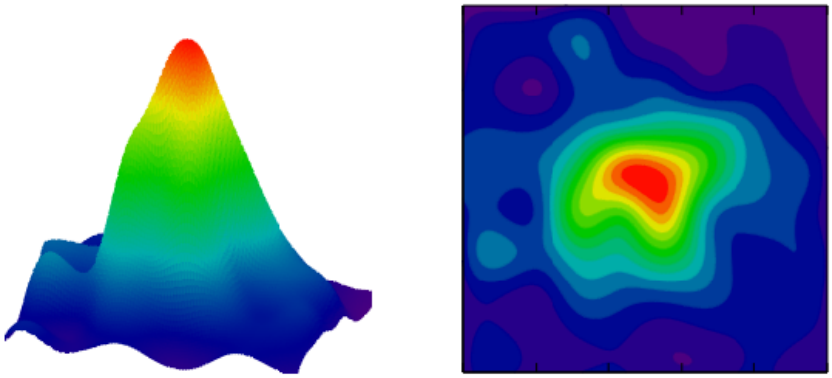

b)

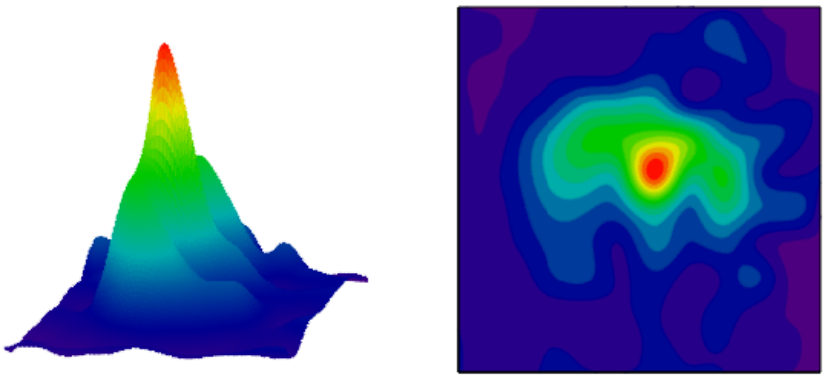

c)

Figure 6.13 - Beam Intensity profiles obtained from different Laser Powers, a) 10 W, b) 20 W, and c) 30 W

Figure 6.14- Burn patterns of laser beam on wood for 10W, 20 W and 30 W

From beam profiling it is possible to conclude for the transverse electromagnetic mode content of laser beam. In the design part it was desired to operate in TEM_{00}+TEM_{01} and this mode should be satisfied by the profiles obtained. Theoretical intensity distribution is given by equation (4.1) and ***Fig. 4.1*** depicts the 3-D plots for different modes separately. But in time of operation it is not possible to separate these modes and the result is their sum. In ***Fig. 6.15*** two dimensional plots of intensity distributions of TEM_{00}, TEM_{01} and their sum is given. As it is seen form the graph it is difficult to distinguish from a single profile the mode of operation since the intensity distributions of TEM_{00} and the sum TEM_{00}+TEM_{01} are nearly the same. Only the top of the sum is flat which means that in the profile we should have a larger red spot in comparison to a TEM_{00} beam. Any measurement on TEM_{00} beam was not carried out and we can not conclude on the mode content of the beam with experimental results. But our theoretical calculation results indicate that considering curvature of the end mirror, resonator length and laser tube diameter we should have obtained a beam with mode content which is the sum of first two transverse electromagnetic modes.

The intensity distribution of a beam is of great importance in material processing. Since the intensity profile of the beam is conserved in the focus point it is important to locate the point of maximum intensity on the axis of propagation that is in the center of the beam. In material processing the region or line that is desired to cut, weld or heat treated is placed on the axis of beam propagation.

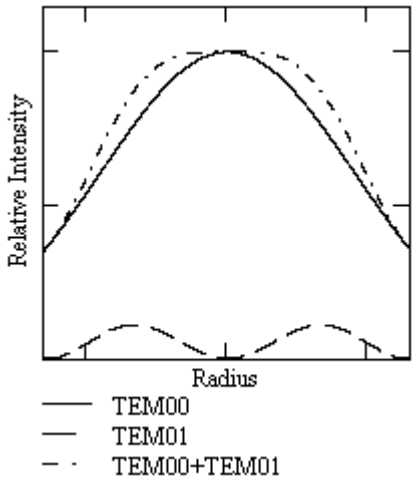

Figure 6.15 -Radial Intensity distribution for TEM_{00}, TEM_{01} and sum TEM_{00}+TEM_{01}

Also the profile should posses a distribution such that points having equal magnitude of intensity should be located in equal distance around the point having maximum intensity, i.e. beam should have a circular cross-section. If this condition is not satisfied the path of processing could not be located properly.

6.2.2- Beam Propagation Parameter and Divergence

The two most important parameters that characterize the laser beam are its beam propagation factor, i.e. beam quality, and divergence. To determine these parameters a lens of known focal length is used to focus the out coming laser beam and by knife edge method beam cuts are made on both sides of focus point to determine the place and size of the beam waist. Setup of the experiment is given in ***Fig. 6.16***. At each cut point diameters are measured in two directions. This allows to observe the difference in beam propagation along the two transversal axis, x and y.

For a beam with acceptable characteristics it is expected to have the same properties in both directions.

To determine the desired properties at twelve points on the propagation path of the focused beam knife edge cuts were made and diameter of the beam at each cut was determined. In Appendix IV use of knife edge cut method is described and a sample calculation is given. Calculated beam diameters are plotted with respect to z-axis in ***Fig. 6.17***.

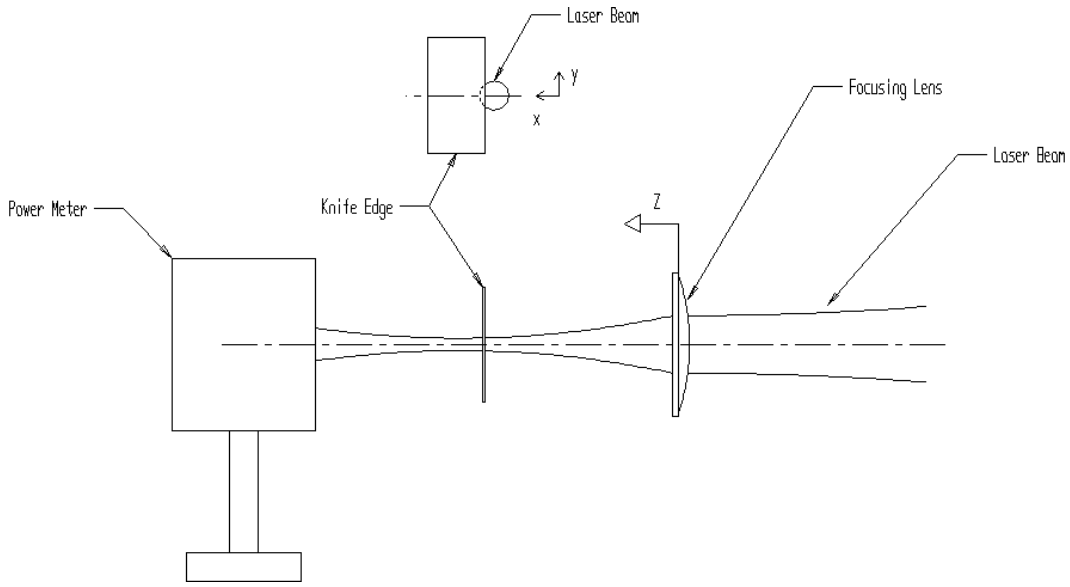

Figure 6.16 - Experimental Setup for knife edge method

A laser beam posses the form of propagation of the equation (4.2). Diameters determined by knife edge method should be fitted to equation (4.2). Since our beam is not purely Gaussian beam it is expected the beam to deviate by a factor equal to the beam quality of the beam. So equation (4.2) is modified such that include the beam propagation factor as well. The modified equation is given below

$$2W(z) = 2W_o\left(1+\left(\frac{4M^2\lambda\left(z-z_o\right)}{\pi\left(2W_o\right)^2}\right)^2\right)^{\frac{1}{2}} \tag{6.1}$$

Since parameters z_o, $2W_o$ and M^2 are not known exactly a trial and error approach was applied in order to fit the equation. For the three unknown parameters a range was specified and equation (6.1) was calculated at data points. The results are determined by estimating the minimum difference between the calculated and measured diameters at data points. At minimum total error the beam waist, its location and beam quality were determined. A plot of the fitted curve for 10 W beam is given in ***Fig. 6.17***.

Curve fitting process was applied for three beams with power of 10W, 20 W and 30 W for two directions and totally six waist diameters and beam quality parameters were determined. From the curves approximating the propagation of the beam, which beam diameters at twelve points along the propagation path were obtained, Rayleigh range for each beam was estimated. By using the beam waist diameter and the Rayleigh range for that beam the divergence for each beam were also calculated. By using the previously measured beam diameters on the focusing lens and calculated beam propagation factors theoretical beam diameters at focal point of the lens were obtained. Also beam focal depth for each beam was calculated. Results of Laser beam properties are given in Table 6.1. A sample calculation for curve fitting and calculation of other beam parameters is given in Appendix-V.

In previous section intensity profiles of beams were determined and it was observed that beams are elliptical. This result was confirmed by the diameter measurements of beams on the lens. This beam ellipticity was conserved through all path of propagation after beam passes focusing lens. From ***Fig. 6.17*** this result can be easily observed. As a result of beam ellipticity different results of beam properties for the different axis of each beam were observed. Due to this observed beam shape evaluation of the results will be done with respect to a given axis at all three power levels.

As general result we can conclude that our beams are of TEM_{00} mode with a small contribution of second TEM_{01} mode since average M2≅1.07. This result is consistent with the plot in ***Fig. 6.15***, that is the area below the curve of TEM_{01} is much less than the area below the curve of TEM_{00} mode.

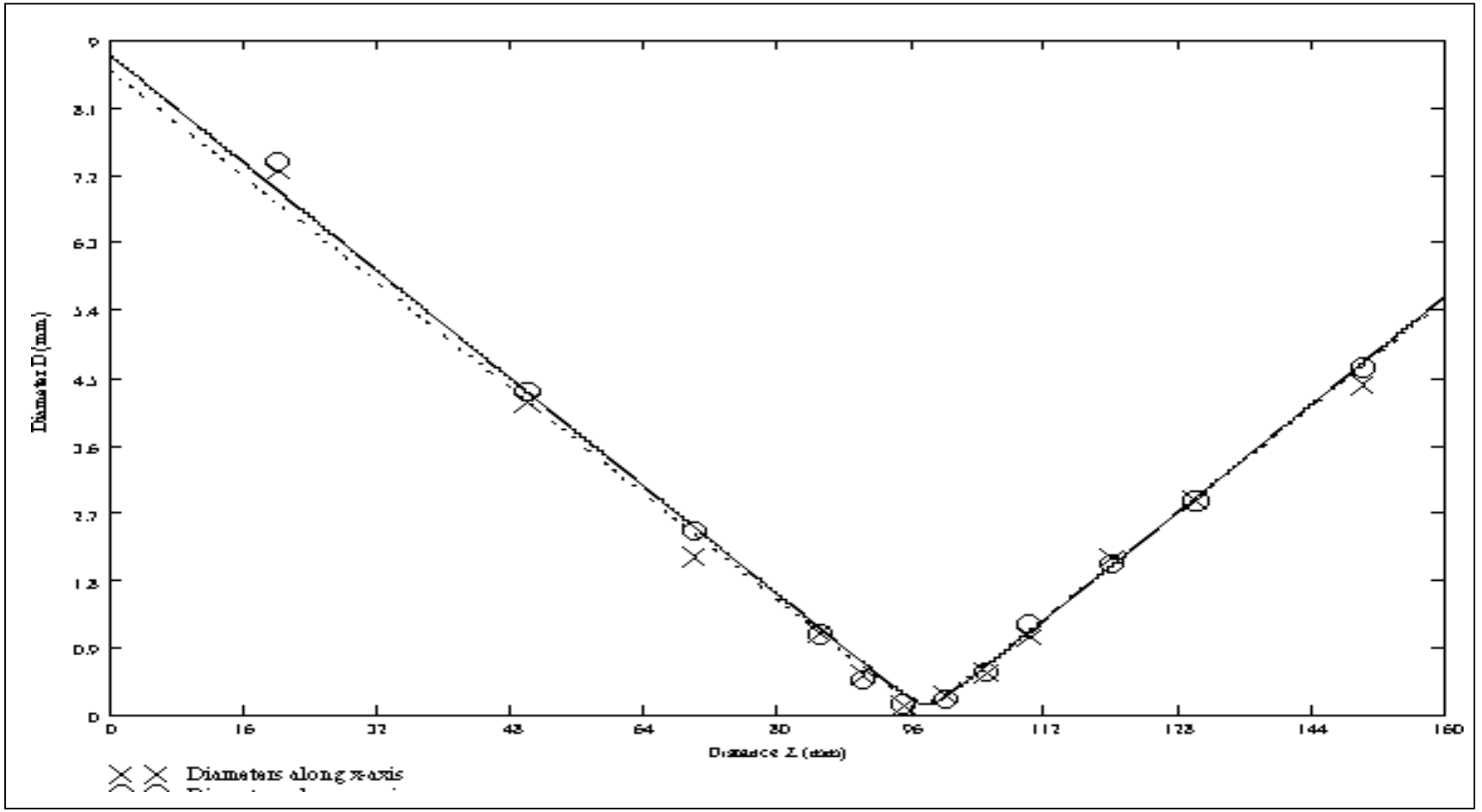

Figure 6.17 - Curve fitted to data of 10 W laser Beam

Table 6.1- Results on Laser Beam Properties

Beam Power	Axis	Beam Diameter on the Lens (mm)	Beam Diameter at focus (mm)	Theoretical Diameter at focus (mm)	Rayleigh Range (mm)	Position of minimum waist (mm)	Beam Divergence (mrad)	Beam Propagation Factor	Focal Depth (mm)
10 W	X-axis	9.030	0.168	0.167	1.908	97.250	88.307	1.103	0.853
	Y-axis	8.700	0.153	0.160	1.700	97.750	89.984	1.020	0.760
20 W	X-axis	8.570	0.164	0.179	1.763	98.500	92.749	1.124	0.788
	Y-axis	9.350	0.143	0.152	1.446	97.500	98.537	1.040	0.647
30 W	X-axis	8.690	0.153	0.163	1.678	96.000	91.537	1.040	0.750
	Y-axis	9.940	0.147	0.153	1.442	97.500	101.568	1.103	0.645

Comparing the beam diameters determined from the curve fitting at focal point and calculated theoretical diameters they are consistent and calculated diameters are slightly lager (+ 0.01 mm) than that determined by curve fitting.

Waist position compared for each beam is different both axes. From this result we can conclude that the beam posses a slight astigmatism.

Comparing the Rayleigh range of beams in one direction(x or y) its observed that it decreases with increasing power. But beam divergence on the other hand increases with increasing power. Behavior of beam propagation factor is the same as beam divergence it increases with increasing power. Focal depth in contrast to beam divergence and beam propagation factor decreases with increasing power. The increase in beam divergence and beam propagation factor and the decrease in Rayleigh range and focal depth indicate the same result, beam is getting worst with increasing power.

The results of different beam properties on different axis of evaluation are the result of worst alignment but differences are less than 10 % and that difference is acceptable.

6.3 – Experiments on Material Processing

The possibility of material processing with the designed laser was investigated. Since the laser output power is low (only 30 W) it is difficult to find a wide application area in material processing. So during the thesis work concentration was made on materials that absorb 10.6 μm wavelength radiation. These materials are Teflon, Plexiglas, pyrex glass and packing paper. Also an attempt was done to cut stainless steel thin sheet of 0.05mm. Primary processing considered was cutting and any work on process optimization was not in the scope of this work.

Laser beam delivery system and nozzle were designed by the author and used in the applications. A photo of the beam delivery unit and a technical drawing of the nozzle are given in Appendix VI.

Cutting of three non metal materials was successful these materials are teflon, pleksiglas and paper.

Thickness of teflon used in experiment was of 4 mm and cuts of 2 mm in depth were realized. During the cutting of teflon there was a little flame and exhaust was not melt but snow like powder. In processing of teflon the cutting mechanism may be chemical bond breaking primarily and very little evaporation which results in flame during the processing. In ***Fig. 6.18a*** a photo taken during the cutting of teflon is shown and two cuts on the sample are also given in ***Fig. 6.18b***.

Attempt to cut a hard 3 mm thick paper was done. It was successful but the speed of cutting was very low 9 cm/min. In paper cutting mechanism was burning there was no melting no vaporization. A performed cut is given in ***Fig. 6.18c***.

5 mm thick pleksiglas was cutted very successfully. The cutting mechanism was vaporization and there was not any melt on the plate. The cut width was measured to lager than 0.1mm but less than 0.15 mm. A photo of the cut is given in ***Fig. 6.18d***.

Also cutting of 1 mm pyrex glass was performed but it was unsuccessful. During the cutting operation glass was broken into pieces in one trial but in the other cut was performed but glass melts were solidified at the edge of the cut. This indicates that the process is not optimized and there is a possibility to cut this material. Cutting mechanism in glass cutting is crack propagation and melting of the material is not allowed. With good cooling during the processing, glass can be successfully cutted.

Possibility of cutting highly reflective materials such as stainless steel was also investigated and with a proper gas selection and processing speed optimization cutting of a 0.05 mm thick material can be performed. In ***Fig. 6.18e*** photo taken during the processing of steel is given. The flame is bright and likes the one in welding applications and this flame indicates the melting of material. In ***Fig. 6.18f*** the cut performed on the stainless sheet is given. As it is observed very clearly heat affected zone around the cut is nearly two times large than the cut width. This result shows that cooling of the sample during the processing was not enough. During processing N_2 gas was used but by using a gas with high heat conduction constant or by use of reactive gas such as oxygen better cuts can be obtained.

a)

b)

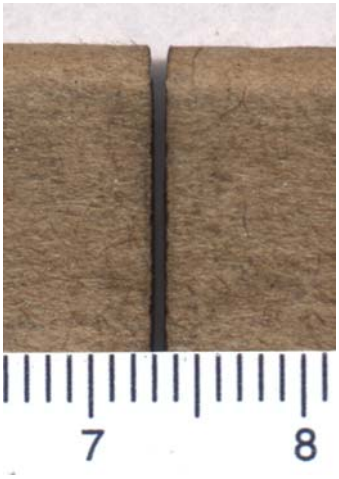

c)

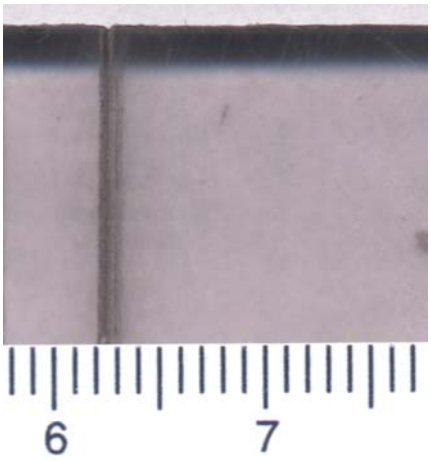

d)

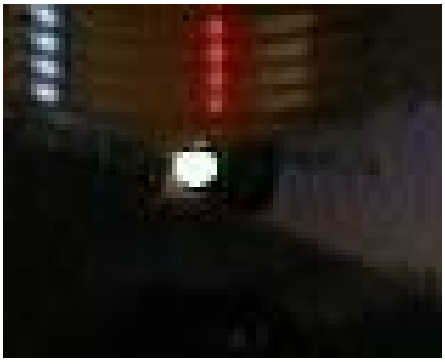

e)

f)

Figure 6.18 - Processed materials; a) Teflon processing, b) Teflon processed, c) Paper processed, d) Cut performed in plexiglas, e) Stainless steel processing, d) Processed stainless steel sheet.

CHAPTER 7

DISCUSSION and CONCLUSION

The main aim of this work was to get experience with the basic structure of CO_2 laser resonators and to get basic understanding of lasing processes. Beside these also laser beam characterization, laser beam guiding and laser beam material processing were the secondary subjects worked on.

The two basic problems of laser resonators are their mechanical and electrical stability. The design realized was faced with both of the problems. Realization of discharge at both tubes was not possible either by using single or two separate power supplies. By using single supply connected to both tubes results in discharge in a single tube completely randomly. By using two separate supplies also results in discharge in a single tube. Second discharge is obtained between the anodes of the resonator and not between the anode and cathode of the second tube.

Although some mechanical solutions for the problem exist during the work electrical solutions were considered. Using of SCR`s group was the solution worked on but it was successful only at pressures below 3 torr. The problem needs further investigations and during the experimental part only one tube was operated.

The mechanical stability of the resonator was another problem faced with. Due to frequent pressure changes fasteners of the mirrors are loosen and this destroys mirror alignment. During the work bending mirrors were stabilized by locking of fasteners but end mirror and output mirror were not stabilized since adjusting micrometer screws were used.

The output power obtained was maximum 32 watts and this result is very far from the design power of 225 watts even if two tubes were in operation. Main reason of that result was the length between the anode and cathode. It is known that small signal gain of a discharge decreases with the increase of length between anode and cathode [27]. Keeping discharge length constant and increasing the anode-cathode pairs is a way to increase the output power of the laser.

Operational experiments of the design were performed considering gas composition, gas pressure and electrical feeding. Results consistent with general relations obtained in previous works [12] [14] were obtained. Since all of such experiments are not performed in maximum operation power or resulting in that power, these results should be evaluated in qualitative manner rather than in quantitative.

Experiments related with beam properties are performed by basic methods although there are available instruments performing such measurements. Beam profiling was performed by pinhole measurements and the size of the pinhole may be critical in evaluation of the results. To minimize the effect of pinhole size on the results 2D curve fitting was applied. This method was used to interpolate the values of points that are not measured between the points that are measured. From obtained profiles it was observed that the beam possess shape of ellipse rather than a circle and this result is a consequence of bad alignment. Beam profiling was performed for three different operational powers and the ellipticity was observed to increase with increase in beam power. This increase may refer to either bad alignment or to the destruction of discharge uniformity with increasing power. Further investigations of the results should be performed.

Beam propagation factor and beam divergence were obtained by curve fitting to data obtained from beam diameter measurements at both sides of the focus point of a focused beam. Twelve diameters were measured for a beam and modified Gaussian beam diameter function with respect to distance traveled were fitted to these data. Curve fitting was done in regard to minimize the error of diameters at data points between the calculated diameters from fitted curve and measured diameters. From the fitted curve beam propagation factor, beam divergence, Rayleigh range for the focused beam, focused beam diameter and focal depth of the

laser beam were obtained. Beam diameters at focal point of the lens were compared to the theoretically calculated beam diameters. Diameter measurements were performed for three beams with different power and for two axes in the cross-section of a cut. So six different sets of beam parameters were obtained and compared. Ellipticity of beams was observed also through diameter measurements and this beam cross-section shape shows his effects on the beam properties. These effects were different divergence and beam propagation factor for each axis of a given power beam.

Possibility of the designed laser to be used in material processing was also investigated at end of the work. Primarily materials that absorb 10.6 mm wavelength radiation were considered. Fine cuts were obtained in paper, teflon and plexiglas. Also it is possible to cut stainless steel if process is optimized. Range of materials that can be processed with 30 W laser can be extended by further investigations. During the work only cutting process was studied and any process optimization work was not carried out. To settle down the application area of such an instrument process optimization and economical effectiveness of the process need to work on.

REFERENCES

1. Patel C.K.N. ,1964, Physical Review Letters, V12, pp. 588
2. Patel C.K.N. 1964, Physical Review Letters, V13, pp. 617
3. Patel C.K.N. 1964, Physical Reviews, V136, A1187
4. Patel C.K.N. 1965, Physical Review Letters, V17, pp. 15
5. Roberts T.G., Hutcheson G. J., Ehrlich J.J., Hales W.L., Barr T.A., 1967, IEEE Journal of Quantum Electronics, V3, pp 605-609
6. Bealieu A.U. 1970, Applied Physics Letters, V16, pp. 504
7. Festermacher C.A., Nutter, M.J., Rink, J.P., Boyer, K. 1971, Bulletin of American Physical Society, V16, pp.42
8. Seguin H.J., Tulip, J., 1972, Applied Physics Letters, V21, pp.414
9. Deutch T.F., Horrigan, F.A., Rudko, R.I., 1969, Applied Physic Letters, V15, pp.88
10. Cool T.A., Shirley, J.A., 1969, Applied Physic Letters, V14, pp70
11. Tiffany W.B., Targ, R., Foster, J.D., 1969, Applied Physic Letters, V15, pp.91
12. Antropov E.T., Silin-Bekchurin, I.A., Sobolev, N.N., Sokovikov, V.V., 1968, IEEE journal of Quantum Electronics, V4, pp.790
13. Matrhews S., 2001, Laser Focus World, V37, pp.185
14. Cheo P.K.,1967, IEEE Journal of Quantum Electronics,V3, pp.683
15. Tyte D. C.,1970, In `Advances in Quantum Electronics` (D.W. Goodwin, ed.), Vol. 1, Academic Press, New York
16. Ballik E.A., Garside, B.K., Reid, J., Tricker, T.,1975, Journal of Applied Physics, Vol. 46, pp. 1322
17. Rigrod W. W.,1965, Journal of Applied Physics, V34, pp. 2487
18. Taylor R.L., Bitterman, S.,1969, Review of Modern Physics, V41, pp.26

19. Fowler M.C., 1972, Journal of Applied Physics, V43, pp. 3480
20. Menzel Ralf, 2001, Photonics- Linear and Nonlinear Interactions of Laser Light and Matter, Springer-Verlag, Berlin,
21. Kogelnik H. , Li, T., 1966, Proceedings of the IEEE, pp. 97
22. Jenkins F.A., 1976, Fundamentals of Optics, 4th Ed., McGraw-Hill, Tokyo,
23. Koechner W., 1999, Solid State Laser Engineering, 5th Ed., Springer-Verlag, Berlin,
24. Weber M. J., 2002, Handbook of Optical Materials, 1st ed., CRC Press, New York
25. Callister W.D., 1997, Materials Science and Engineering: an Introduction, 4th ed., John Willey & Sons, New York
26. Welch M., Lasers&Applications , 1986, pp.67-71
27. Bogaerts A., Grozeva, M., 2002, Applied Physics B, V75, pp.731-738
28. Sherman Glen F., Danielewicz, Edward J., Rudisill, J.Earl, Lasers & Optronics, September 1988

APPENDIX I

LASER DESIGN CALCULATIONS

A1.1 - Laser Output Parameters

$P_{out} := 225W$

$\theta := 2 \cdot 10^{-3} rad$

TEM_{00} + TEM_{01}* mode of operation

A1.2 - Slow flow laser power constants

$p_{00} := 50 \frac{W}{m}$ for laser operation in TEM_{00} mode

$p_{01} := 75 \frac{W}{m}$ for laser operation in TEM_{00} + TEM_{01}*mode

A1.3 - Calculation of Discharge and Resonator Lengths

A1.3.1- Discharge Length

$L_d := \frac{P_{out}}{p_{01}}$ $L_d = 3\,m$

A1.3.2- Optical Length

$L := 1.25 \cdot L_d$ $\quad L = 3.75\text{m}$

A1.4 - Calculation of mirror radii

A1.4.1-Curvature of End Mirror

$\lambda := 10.6\mu\text{m}$

$w_o := \frac{2 \cdot \lambda}{\theta \cdot \pi}$ $\quad w_o = 3.374\text{mm}$

$R_2 := \left(w_o^2 \cdot \frac{\pi}{\lambda} \right)^2 \cdot \frac{1}{L} + L$ $\quad R_2 = 6.786\text{m}$

A mirror with larger value that is in hand is selected

$R_2 := 8\text{m}$

A1.4.2 - Curvature of Output Mirror

Resonator type is hemispherical and the output coupler is plane.

$R_1 := 10^{20}\text{m}$ (i.e. plane)

A1.5- Stability of The Resonator

$g_1 := 1 - \frac{L}{R_1}$ $\quad g_2 := 1 - \frac{L}{R_2}$ $\quad g_1 \cdot g_2 = 0.531$ $\quad 0 < g_1.g_2 < 1$

A1.6- Beam diameters on mirrors

A1.6.1- Output Beam Diameter for Fundamental Mode

$w_o := \left[\frac{\lambda}{\pi} \cdot \sqrt{L \cdot (R_2 - L)} \right]^{\frac{1}{2}}$ $\quad D_o := 2 \cdot w_o$ $\quad D_o = 7.3\text{mm}$

A1.6.2-Beam Diameter on the End Mirror for Fundamental Mode

$$w_e := \left[\left(\frac{\lambda \cdot R_2}{\pi} \right)^2 \cdot \frac{R_1 - L}{R_2 - L} \cdot \left(\frac{L}{R_1 + R_2 - L} \right) \right]^{\frac{1}{4}} \qquad D_e := 2 \cdot w_e \qquad D_e = 10.1\,\text{mm}$$

A1.6.3 - Mode Content of Resonator

$$C := \begin{pmatrix} 1 & 1.5 \\ 1.9 & 2.15 \\ 2.42 & 2.63 \end{pmatrix}$$ Mode Coefficients [23]

Laser TEM mode abbreviations

$$TEM := \begin{pmatrix} 00 & 01 \\ 10 & 11 \\ 20 & 21 \end{pmatrix}$$

A1.6.3.1 - On output mirror

$$D_o := 2 \cdot C \cdot w_o \qquad D_o = \begin{pmatrix} 7.3 & 11 \\ 13.9 & 15.8 \\ 17.8 & 19.3 \end{pmatrix} \text{mm}$$

A1.6.3.2 - On end Mirror

$$D_e := D_o \cdot \sqrt{\frac{g_1}{g_2}} \qquad D_e = \begin{pmatrix} 10.1 & 15.1 \\ 19.1 & 21.7 \\ 24.4 & 26.5 \end{pmatrix} \text{mm}$$

A1.6.4 - Selection of tube diameter

TEM 01 diameter on the output mirror is $D_{o_{0,1}} = 11\,\text{mm}$ and on the end mirror is $D_{e_{0,1}} = 15.1\,\text{mm}$

Selected Diameter : $D_{tube} := 16.4\,\text{mm}$

A1.7- Beam Divergence of the Fundamental Mode

$$\theta := \frac{2\cdot\lambda}{\pi\cdot w_o} \qquad \theta = 1.839\times 10^{-3}\ \text{rad}$$

A1.8 - Transmittance of Output Coupler

A1.8.1 - Mirror Losses

$a_1 := 0.01$ $a_2 := 0.005$ $a_3 := 0.005$ $a_4(\gamma) := \gamma$

A1.8.2 - Mirror Reflectances

$r_1 := 1 - (a_1 + a_2 + a_3)$

All total reflectors are considered as one

$r_2(\gamma, t) := 1 - t - \gamma$

Reflectance of output mirror

A1.8.3 - Calculation of transmittance by Rigrod's method

$$\eta(t, L, g_o, \gamma) := \frac{r_1^{0.5}\cdot t}{\left[r_1^{0.5} + \left(r_2(\gamma, t)\right)^{0.5}\right]\cdot\left[1 - \left(r_1\cdot r_2(\gamma, t)\right)^{0.5}\right]}\cdot\left(1 + \frac{\ln\left(r_1\cdot r_2(\gamma, t)\right)}{2\cdot g_o\cdot L}\right)$$

A1.8.3.1 - Behavior of Rigrods formula for different conditions

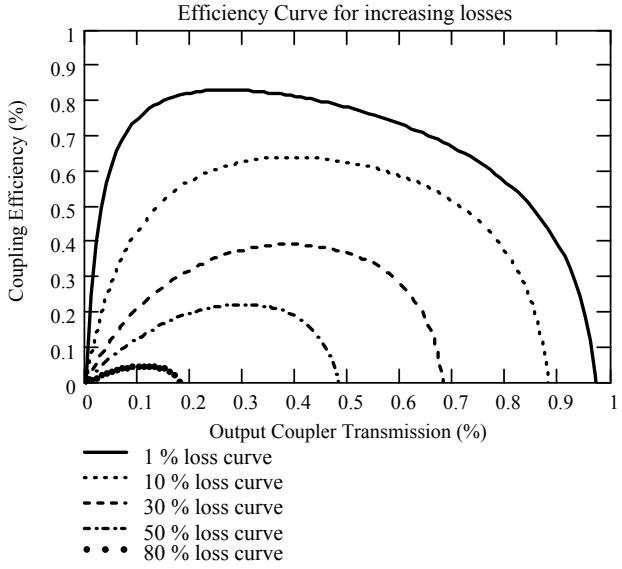

Figure A1.1 - Efficiency Curve for increasing losses

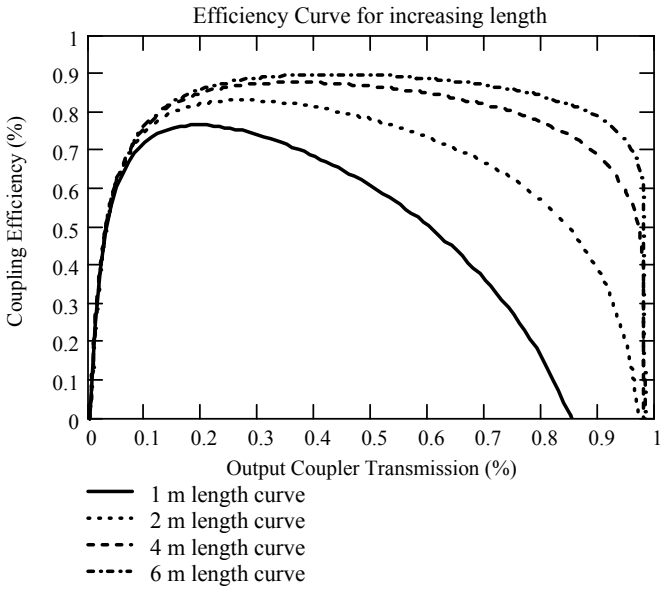

Figure A1.2- Efficiency Curve for increasing length

A1.8.3.2 - Selection of go for transmission calculations

From Fig 5 for a tube with diameter of 16.4 mm and pressure of 4 torr value of 3 was selected.

$\alpha := 3\text{dB}$ $\quad \alpha = -10\cdot\log(g_o)$ $\quad g_o := 10^{\frac{-\alpha}{10}}\cdot\frac{1}{m}$ $\quad g_o = 0.501\frac{1}{m}$

A1.8.3.3 - Efficiency plot and Transmission determination for design

$L_d = 3\,m$ $\quad g_o = 0.501\frac{1}{m}$

γ = increasing

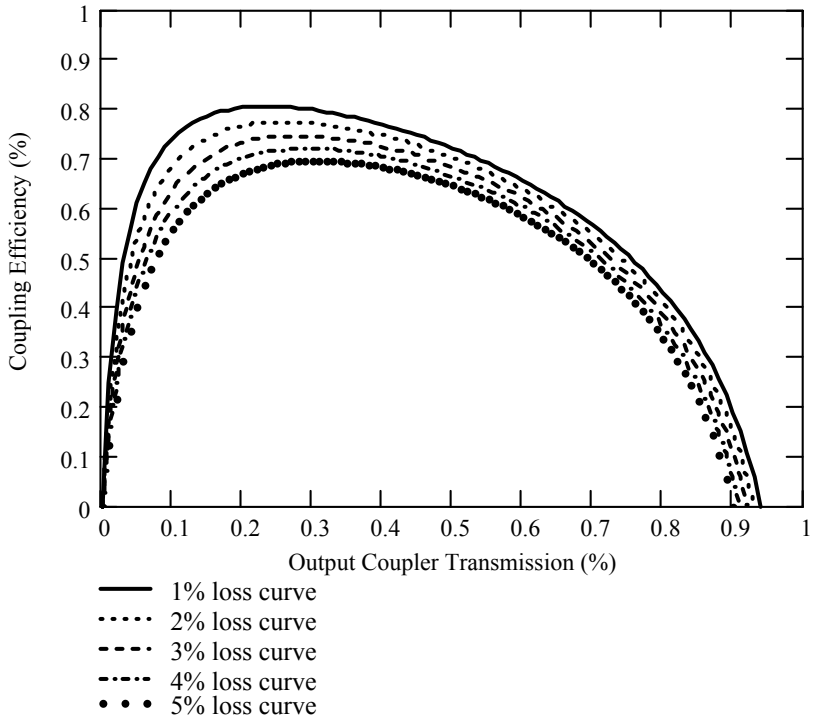

Figure A1.3 - Efficiency Curve for increasing losses of designed laser

$T := 20\%$ is selected for the output transmission

A1.9 - Selection of Mirror Materials

A1.9.1- Output Coupler Material

Table A1.1- Material Properties of possible Output Coupler Material s [24]

Material	Thermal Expansion Coefficient (10^{-6}/K)	Thermal Conductivity (W/m.K)	Thermo Optic Coefficient (10^{-6}/K)
GaAs	5	65	200
Ge	5.7	59.9	401
KCl	36.5	6.7	-34.8
ZnSe	7.1	13	61

Function for figure of merit: $F = \frac{K}{A \cdot X}$

K - Thermal Conductivity ; A - Total Absorption

$X_1 = \frac{d}{dT}L + \frac{d}{dT}n$ Thermal Expansion coefficient + Refractive index gradient

or

$X_2 = \frac{d}{dT}L$ Thermal Expansion

$$F(\psi, A, \Delta L) := \frac{\psi \cdot \frac{m \cdot K}{W}}{A \cdot (\Delta L) \cdot K \cdot 10^8}$$

Figure of Merit Function for thermal Expansion

$$F(\psi, A, \Delta L, \Delta n) := \frac{\psi \cdot \frac{m \cdot K}{W}}{A \cdot (\Delta L + \Delta n) \cdot K \cdot 10^8}$$

Figure of Merit Function for Thermal Expansion coefficient plus Refractive index gradient

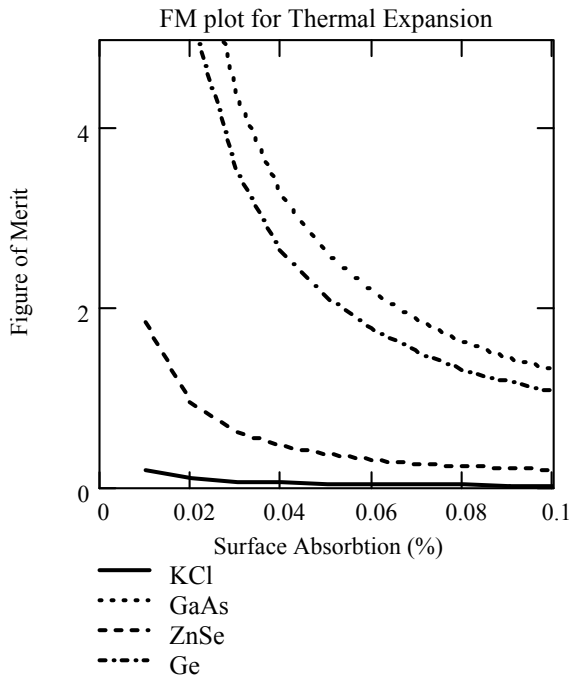

Figure A1.4 - Figure of Merit for Thermal Expansion

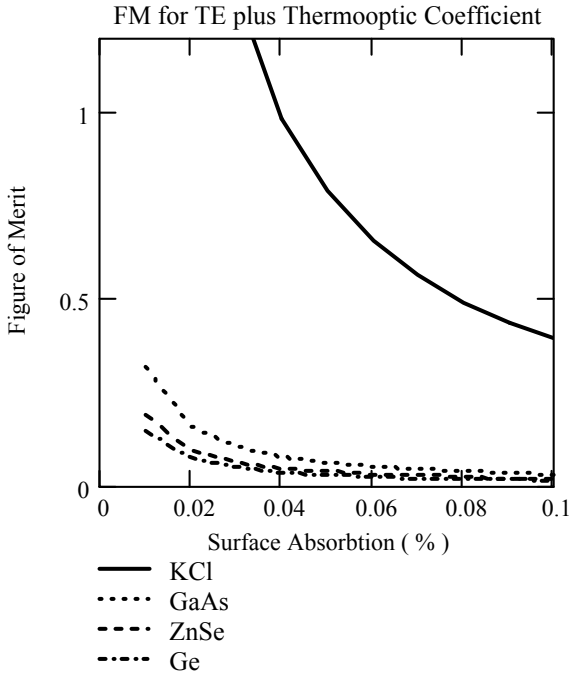

Figure A1.5 - Figure of Merit for Combined Thermal Expansion and Refractive gradient change effect

A1.9.2 - Material Selection for Full Reflector Mirrors

Table A1.2 – Material Properties of Possible Materials for Total reflector mirrors [24]

Material	Thermal Expansion Coefficient (10^{-6}/K)	Thermal Conductivity (W/m.K)
Cu	17	398
Si	4.9	142
Mo	2.5	141

$$F(\psi, A, \Delta L) := \frac{\psi \cdot \frac{m \cdot K}{W}}{A \cdot (\Delta L) \cdot K \cdot 10^{9}}$$

Figure of Merit Function for thermal Expansion

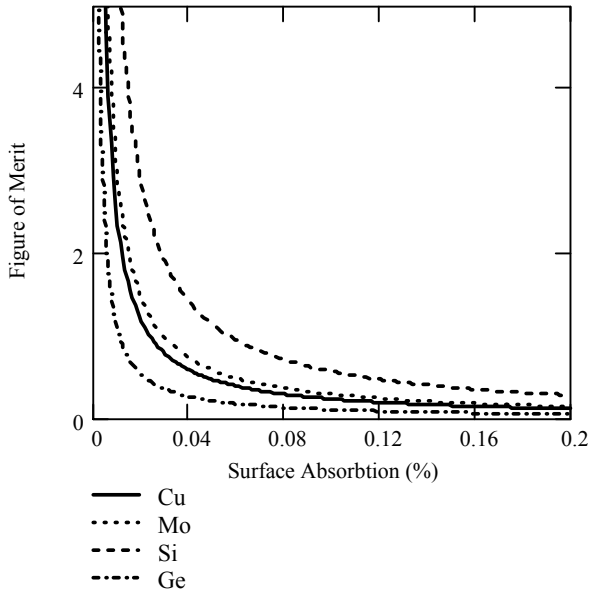

Figure A1.6 - Figure of Merit for Thermal Expansion for total reflection mirrors

APPENDIX II

REALIZED DESIGN AND TECHNICAL DRAWINGS

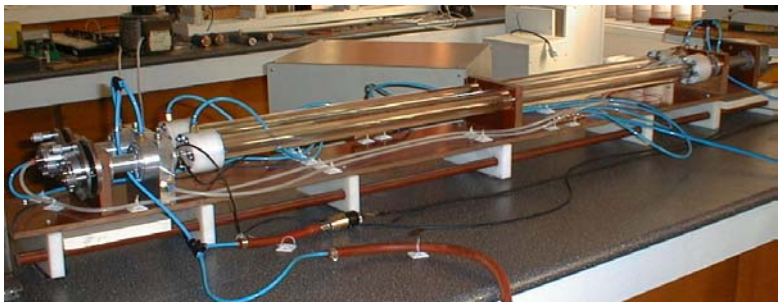

a)

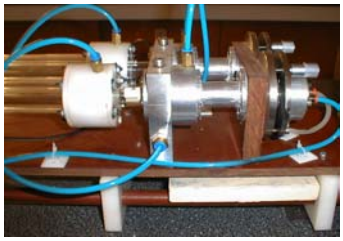

b)

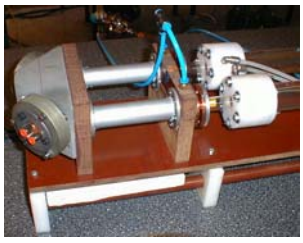

c)

Figure A2.1- Realized design: a) General view, b) Cathode side, c) Anode side

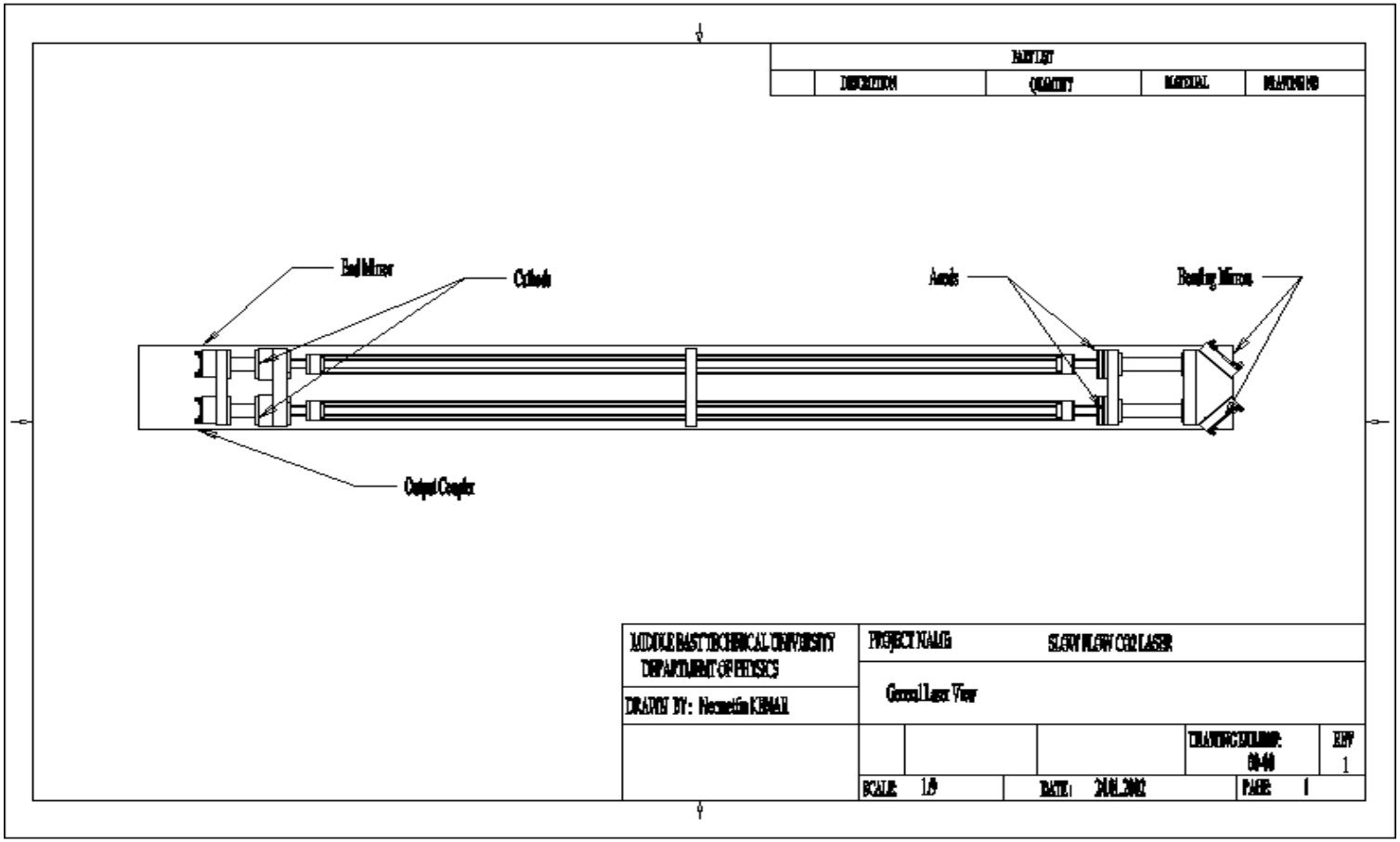

Figure A2.2- General Top view of the Design

Figure A2.3- Cathode side view of the Design

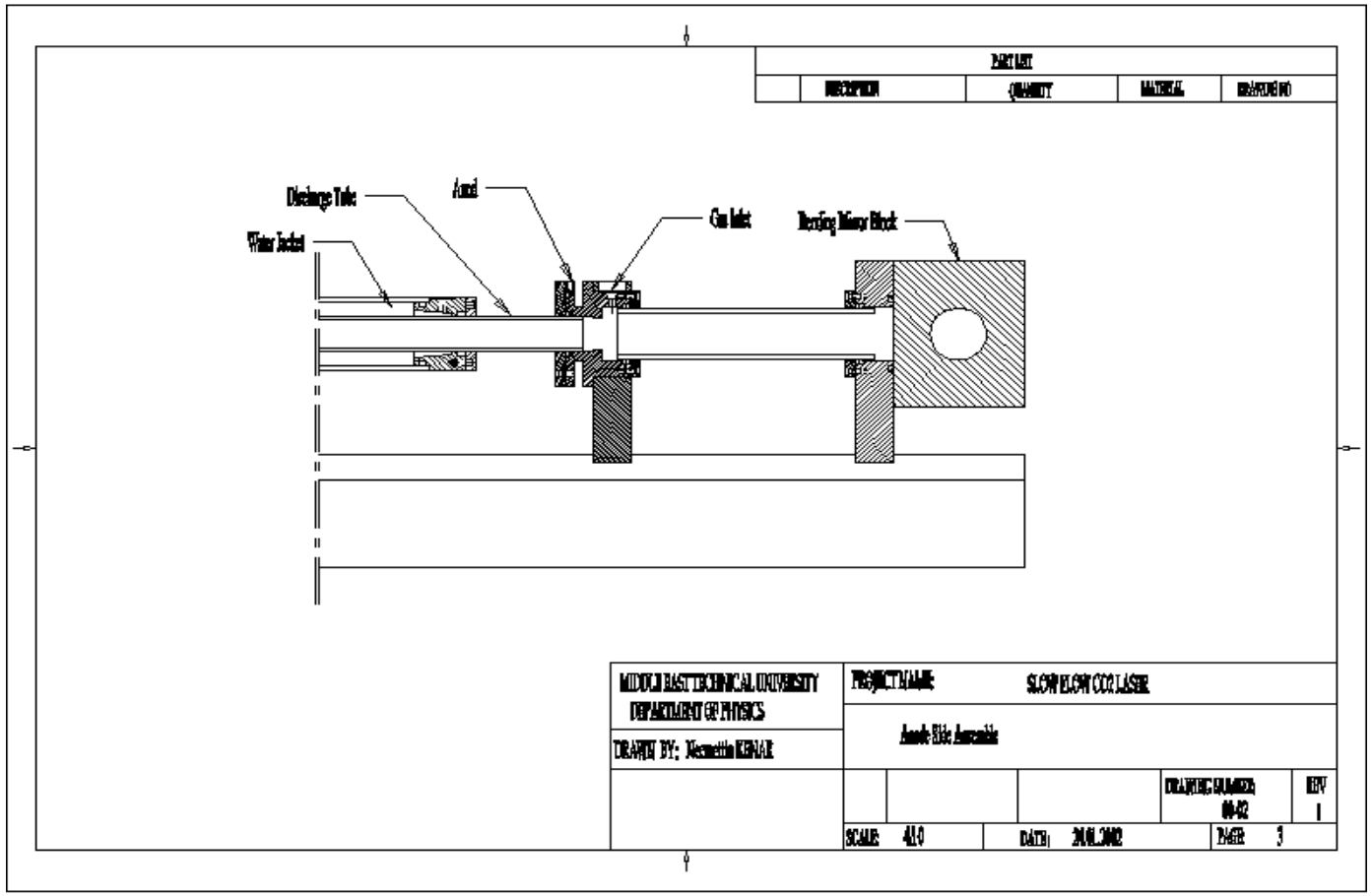

FigureA2. 4- Anode side view of the Design

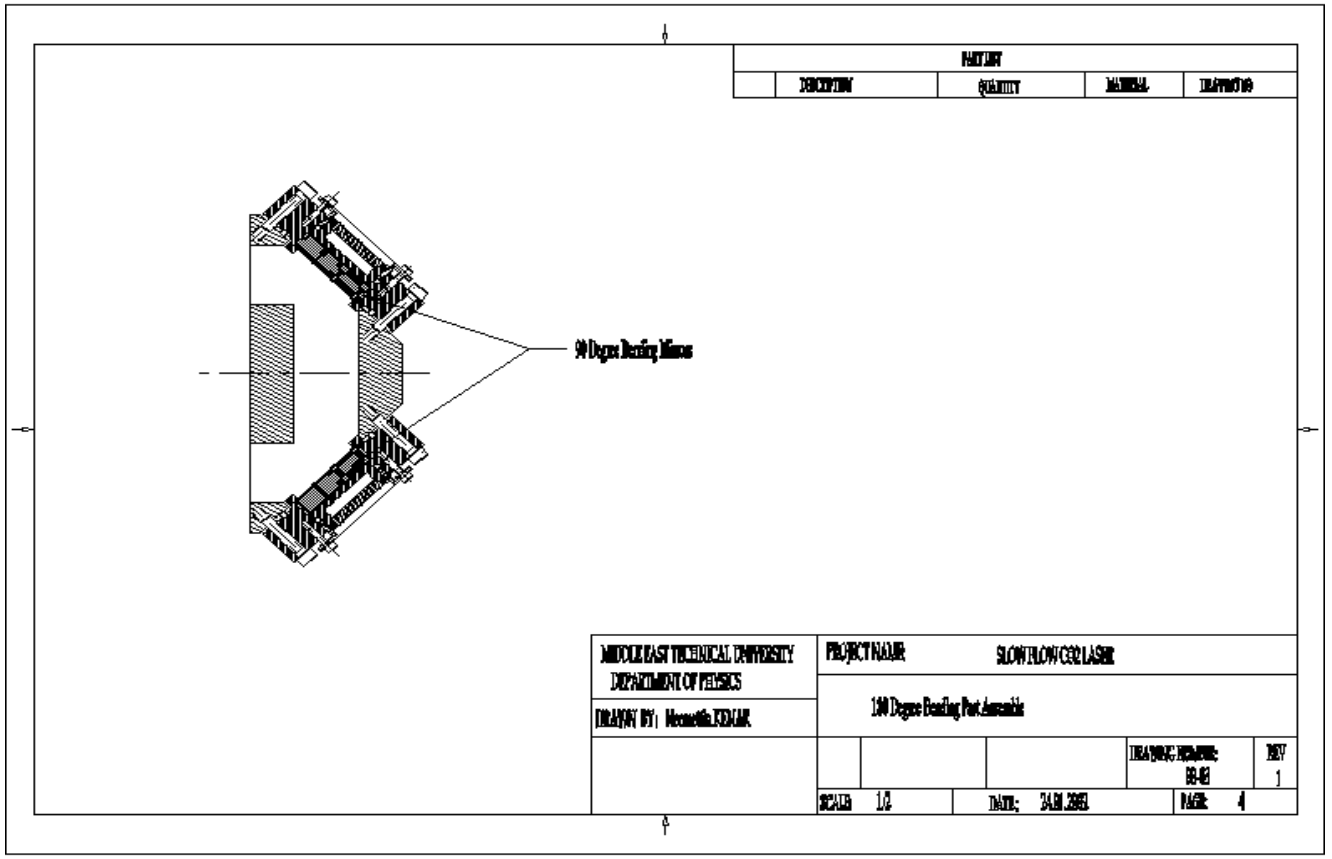

FigureA2. 5- Beam Bending Mirrors Assemble view of the Design

APPENDIX III

BEAM PROFILING

A3.1 - Obtained Data from pinhole power measurements

Data =

	1	2	3	4	5	6	7	8	9	10
1	0.06	0.07	0.07	0.07	0.07	0.06	0.07	0.06	0.05	0.05
2	0.05	0.06	0.06	0.07	0.08	0.07	0.07	0.05	0.04	0.03
3	0.06	0.07	0.07	0.07	0.09	0.1	0.1	0.08	0.05	0.04
4	0.06	0.06	0.07	0.1	0.14	0.15	0.17	0.1	0.06	0.04
5	0.05	0.05	0.06	0.08	0.15	0.2	0.15	0.12	0.07	0.04
6	0.05	0.05	0.05	0.08	0.15	0.23	0.16	0.12	0.08	0.06
7	0.05	0.05	0.06	0.08	0.13	0.17	0.14	0.09	0.07	0.05
8	0.05	0.05	0.06	0.07	0.11	0.12	0.1	0.07	0.07	0.05
9	0.05	0.05	0.05	0.06	0.07	0.08	0.07	0.06	0.06	0.04
10	0.05	0.05	0.03	0.05	0.06	0.05	0.05	0.06	0.06	0.05

W

A3.2 - Data Normalization

Data are normalized to the maximum power measured.

$$M := \frac{Data}{\max(Data)}$$

M =

	1	2	3	4	5	6	7	8	9	10
1	0.261	0.304	0.304	0.304	0.304	0.261	0.304	0.261	0.217	0.217
2	0.217	0.261	0.261	0.304	0.348	0.304	0.304	0.217	0.174	0.13
3	0.261	0.304	0.304	0.304	0.391	0.435	0.435	0.348	0.217	0.174
4	0.261	0.261	0.304	0.435	0.609	0.652	0.739	0.435	0.261	0.174
5	0.217	0.217	0.261	0.348	0.652	0.87	0.652	0.522	0.304	0.174
6	0.217	0.217	0.217	0.348	0.652	1	0.696	0.522	0.348	0.261
7	0.217	0.217	0.261	0.348	0.565	0.739	0.609	0.391	0.304	0.217
8	0.217	0.217	0.261	0.304	0.478	0.522	0.435	0.304	0.304	0.217
9	0.217	0.217	0.217	0.261	0.304	0.348	0.304	0.261	0.261	0.174
10	0.217	0.217	0.13	0.217	0.261	0.217	0.217	0.261	0.261	0.217

A3.3 - 2D Curve fitting

Since obtained data correspond to specified points on the beam cross section, value of surrounding and not measured points can be found by interpolation. For our case 2D cubic spline will be used for curve fitting interpolation function.

$\text{rows}(M) = 10$ $\text{cols}(M) = 10$ $n := \text{rows}(M)$

X and Y n-vectors that determine the mesh for the matrix:

X :=

0
1
2
3
4
5
6
7
8
9

Y :=

0
1
2
3
4
5
6
7
8
9

$Mxy := \text{augment}(\text{sort}(X), \text{sort}(Y))$

$\text{rows}(Mxy) = 10$

Computed spline coefficients:

$S := \text{cspline}(Mxy, M)$

Fitting function for surface:

$fit(x, y) := \text{interp}\left[S, Mxy, M, \begin{pmatrix} x \\ y \end{pmatrix}\right]$ $xlow := Mxy_{1,1}$ $xhigh := Mxy_{n,1}$

$ylow := Mxy_{1,2}$ $yhigh := Mxy_{n,2}$

Density of mesh for interpolation:

$xn := 10 \cdot n$ $yn := 10 \cdot n$ $i := 1 .. xn$ $j := 1 .. yn$

$$xind_i := xlow + i \cdot \frac{xhigh - xlow}{xn} \qquad yind_j := ylow + j \cdot \frac{yhigh - ylow}{yn}$$

Curve Fitting Function: $FIT_{i,j} := fit(xind_i, yind_j)$

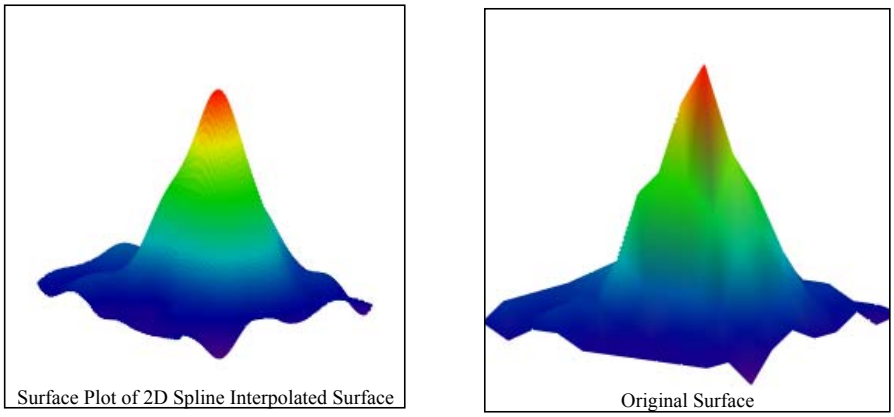

Figure A3.1- 3D surface plot of beam intensity profiler

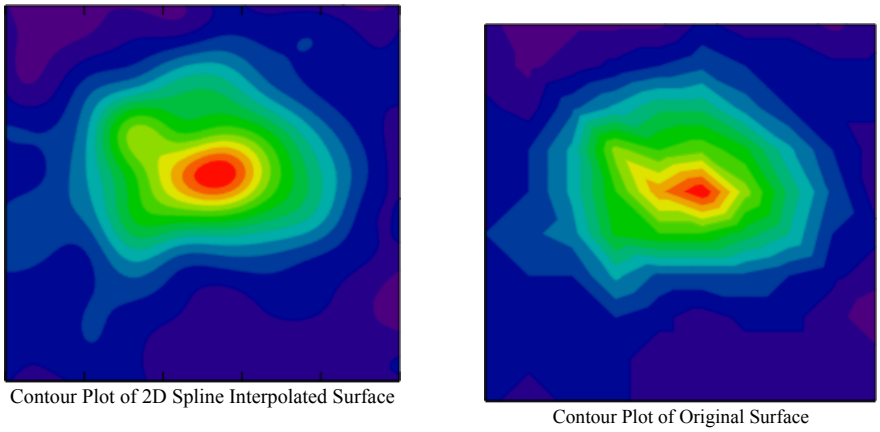

Figure A3.2- Contour plot of beam intensity profiles

APPENDIX IV

KNIFE EDGE METHOD FOR LASER BEAM DIAMETER MEASUREMENTS

A4.1 - Description of Method

A plate with very thin edge (Knife Edge) is placed perpendicularly on the path of propagation of the beam, which diameter is desired to be measured, such that to prevent the beam to pass across the knife edge plate. After that the knife edge plate is pulled out by recording power passing across the edge with respect to distance traveled. Recorded powers are divided by the maximum power recorded and multiplied by one hundred in order to obtain percentage values with respect to the beam total power. Percentage power changes are plotted with respect to traveled distance and distance between %15.9 and % 84.1 is obtained graphically. Two times that distance gives the diameter of the beam. This diameter is equal to the $(1-1/e^2)$ of the diameter of a Gaussian beam.

A4.2 - *Obtained Data*

$a := 0.0254\,mm$ Distance traveled by one step of micrometer screw.

Distance Traveled:

$$X := \begin{pmatrix} 0 \\ 25 \\ 75 \\ 100 \\ 125 \\ 150 \\ 175 \\ 200 \\ 225 \\ 250 \\ 275 \\ 300 \\ 350 \\ 400 \end{pmatrix} \cdot a$$

Power corresponding to traveled distance:

$$P := \begin{pmatrix} 0.77 \\ 1.18 \\ 2.41 \\ 3.45 \\ 4.76 \\ 6.33 \\ 8.59 \\ 10.99 \\ 13.22 \\ 15.35 \\ 17.02 \\ 18.19 \\ 19.59 \\ 20.58 \end{pmatrix} W$$

A4.3 - Data Analysis

$P_c := \left\| \begin{array}{l} \text{for } i \in 1..\text{rows}(P) \\ \quad M_i \leftarrow \dfrac{P_i}{\max(P)} \cdot 100 \\ M \end{array} \right.$	The Loop on the left estimates percentage of transmitted power with respect to total beam power.

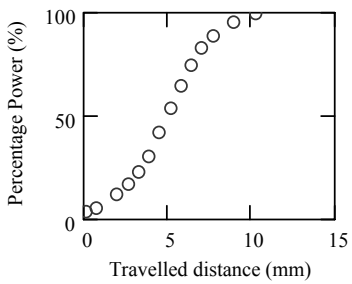

Figure A4.1 - Percentage power as a function of distance traveled.

A4.3.1 - Fitting Cubic Spline to approximate obtained data

Algorithm a Cubic Spline fit in MathCAD®:

$$\text{data} := \left| \begin{array}{l} \text{for } i \in 1..\text{rows}(P) \\ \quad \left| \begin{array}{l} M_{i,1} \leftarrow \dfrac{X_i}{mm} \\ M_{i,2} \leftarrow Pc_i \end{array} \right. \\ M \end{array} \right.$$

$\text{data} := \text{csort}(\text{data}, 1)$ $\quad X := \text{data}^{\langle 1 \rangle}$ $\quad Y := \text{data}^{\langle 2 \rangle}$

Spline coefficients: $S := \text{cspline}(X, Y)$

Fitting function: $\text{fit}(x) := \text{interp}(S, X, Y, x)$

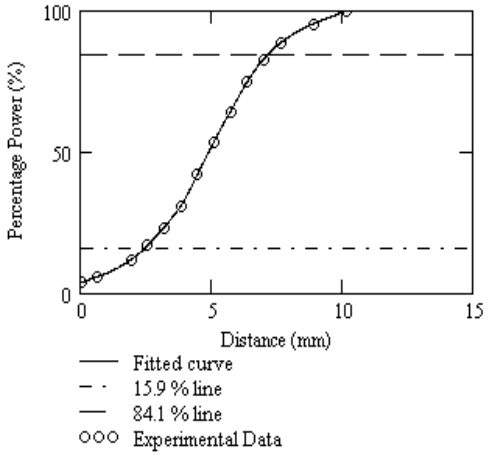

Figure A4.2- Plot of experimental data, Fitted curve and 15.9% and 84.1 % lines as a function of distance.

Beam Diameter:

$D := \left(\left| \text{root}(\text{fit}(x) - 15.9, x, 0, 7) - \text{root}(\text{fit}(x) - 84.1, x, 5, 10) \right| \right) \cdot 2$ $\qquad D = 9.353$

APPENDIX V

DETERMINATION OF BEAM PROPERTIES

A5.1- Experimental Data

Distance from the reference Point	Measured diameters for 10W, 20W, 30 W laser beams in x and y-directions. First, third and fifth columns are diameters measured for x –axis and the others are for y-axis respective to power increasing order

$$Z := \begin{pmatrix} 20 \\ 50 \\ 70 \\ 85 \\ 90 \\ 95 \\ 100 \\ 105 \\ 110 \\ 120 \\ 130 \\ 150 \end{pmatrix} \qquad W = \begin{pmatrix} 7.246 & 7.377 & 8.255 & 7.897 & 7.403 & 8.44 \\ 4.178 & 4.317 & 4.386 & 4.686 & 4.231 & 4.847 \\ 2.111 & 2.451 & 2.63 & 2.639 & 2.248 & 2.64 \\ 1.09 & 1.083 & 0.87 & 1.051 & 0.94 & 1.186 \\ 0.531 & 0.486 & 0.433 & 0.812 & 0.331 & 0.4 \\ 0.137 & 0.146 & 0.067 & 0.255 & 0.175 & 0.113 \\ 0.281 & 0.227 & 0.256 & 0.245 & 0.147 & 0.279 \\ 0.579 & 0.577 & 0.537 & 0.91 & 0.603 & 0.454 \\ 1.039 & 1.219 & 1.161 & 1.263 & 1.215 & 1.281 \\ 2.097 & 2.009 & 2.033 & 2.303 & 2.218 & 2.131 \\ 2.865 & 2.85 & 2.993 & 3.049 & 3.119 & 3.424 \\ 4.411 & 4.628 & 4.602 & 5.136 & 4.929 & 5.286 \end{pmatrix}$$

A5.2 – Derivation of Curve fit Equation

The spot size of a Gaussian beam a distance z from the beam waist expands as a hyperbola, which has the form

$$\omega(z) = \omega_o \left[1 + \left[\frac{\lambda z}{\pi (\omega_o)^2} \right]^2 \right]^{\frac{1}{2}} \qquad \text{(A5-1)}$$

Divergence of Gaussian Beam at far field:

$$\theta = \frac{2\lambda}{\pi \cdot \omega_o} \tag{A5-2}$$

By inserting (A5-2) in (A5-1):

$$\omega(z) = \omega_o \left[1 + \left(\frac{\theta z}{2 \cdot \omega_o} \right)^2 \right]^{\frac{1}{2}} \tag{A5-3}$$

Divergence of a real beam:

$$\Theta = M \cdot \theta \tag{A5-4}$$

Diameter of a real beam at waist:

$$W_o = M \cdot \omega_o \tag{A5-5}$$

Beam Product of a real beam:

$$W_o \cdot \Theta = M^2 \cdot \theta \cdot \omega_o = M^2 \cdot \frac{2 \cdot \lambda}{\pi \cdot \omega_o} \cdot \omega_o \tag{A5-6}$$

Beam Propagation Factor:

$$M^2 = \frac{\pi \Theta (2 W_o)}{4\lambda} \tag{A5-7}$$

By inserting (A5-7) in (A5-3):

$$W(z) = W_o \left[1 + \left[\frac{M^2 \cdot \lambda \cdot z}{\pi (W_o)^2} \right]^2 \right]^{\frac{1}{2}} \tag{A5-8}$$

Replacing $W(z)$ by 2W(z) and W_o by $2 \cdot W_o$ in equation (A5-8)

$$2W(z) = 2W_o \left[1 + \left[\frac{4M^2 \cdot \lambda \cdot z}{\pi (2 W_o)^2} \right]^2 \right]^{\frac{1}{2}} \tag{A5-9}$$

Replacing 2W(z) by W(z) and $2W_o$ by W_o in equation (A5-9) we obtain a function giving beam diameters

$$W(z) = W_o \left[1 + \left[\frac{4M^2 \cdot \lambda \cdot z}{\pi (W_o)^2} \right]^2 \right]^{\frac{1}{2}} \tag{A5-10}$$

and this equation will be fitted to data obtained.

A5.3 - Curve Fitting

Since from obtained data we cannot conclude on waist diameter, location of waist and beam quality factor a simple approach is to define a range for these constants and to calculate equation (A5-10) over that range at data points and to minimize the error between calculated and obtained beam diameters. The constants for which the errors between calculated and measured results are minimum are the parameters of our beam.

Range for z_o : $90..110$

Range for W_o : $\frac{1}{2}\cdot\min\left(W^{\langle column\_number\rangle}\right)..4\cdot\min\left(W^{\langle column\_number\rangle}\right)$

Range for M : $1..2.5$

Curve fitting Function:

$$\omega(x, w_o, z_o, M) := w_o\cdot\left[1+\left[\frac{4\cdot M^2\lambda\cdot(x-z_o)}{\pi\cdot(w_o)^2}\right]^2\right]^{\frac{1}{2}} \qquad \text{(A5-11)}$$

Minimum Error Loop:

```
I := | for j ∈ 1..cols(W)
     |   err ← 10
     |   for φ ∈ 0.5·min(W^⟨j⟩), (0.5·min(W^⟨j⟩) + 0.01)..4·min(W^⟨j⟩)
     |     for υ ∈ 90, 90.25..110
     |       for τ ∈ 1, 1.01..5
     |         ror ← Σ_{i=1}^{rows(Z)} [ | (W^⟨j⟩)_i − ω(Z_i, φ, υ, τ) | ]
     |         if err > ror
     |           U_{1,j} ← φ
     |           U_{2,j} ← υ
     |           U_{3,j} ← τ
     |           err ← ror
     |           err
     |         err
     | U
```

Loop Results:

$$I = \begin{pmatrix} 0.168 & 0.153 & 0.164 & 0.143 & 0.153 & 0.147 \\ 97.25 & 97.75 & 97.75 & 97.5 & 96 & 97.5 \\ 1.05 & 1.01 & 1.06 & 1.02 & 1.02 & 1.05 \end{pmatrix}$$

A5.4 - Beam Constants

A5.4.1- Waist Location

$z_{o_j} := I_{2,j}$

$$z_o = \begin{pmatrix} 97.25 \\ 97.75 \\ 97.75 \\ 97.5 \\ 96 \\ 97.5 \end{pmatrix}$$

A5.4.2- Rayleigh Range for each beam

$$Z_{R_j} := \frac{\left| I_{2,j} - \text{root}\left(\omega\left(x, I_{1,j}, I_{2,j}, I_{3,j}\right) - \sqrt{2}\cdot I_{1,j}, x, I_{2,j}, 160\right)\right| + \left| I_{2,j} - \text{root}\left(\omega\left(x, I_{1,j}, I_{2,j}, I_{3,j}\right) - \sqrt{2}\cdot I_{1,j}, x, 50, I_{2,j}\right)\right|}{2}$$

$$Z_R = \begin{pmatrix} 1.908 \\ 1.7 \\ 1.763 \\ 1.446 \\ 1.678 \\ 1.442 \end{pmatrix}$$

A5.4.3 - Beam Propagation Factor

$M_j := \left(I_{3,j}\right)$

$$\left(M_j\right)^2 = \begin{pmatrix} 1.103 \\ 1.02 \\ 1.124 \\ 1.04 \\ 1.04 \\ 1.103 \end{pmatrix}$$

A5.4.4 - Beam Divergence

$\Theta_j := \dfrac{I_{1,j}}{Z_{R_j}}$

$$\Theta_j = \begin{pmatrix} 88.3 \\ 90 \\ 92.7 \\ 98.5 \\ 91.5 \\ 101.6 \end{pmatrix} \text{mrad}$$

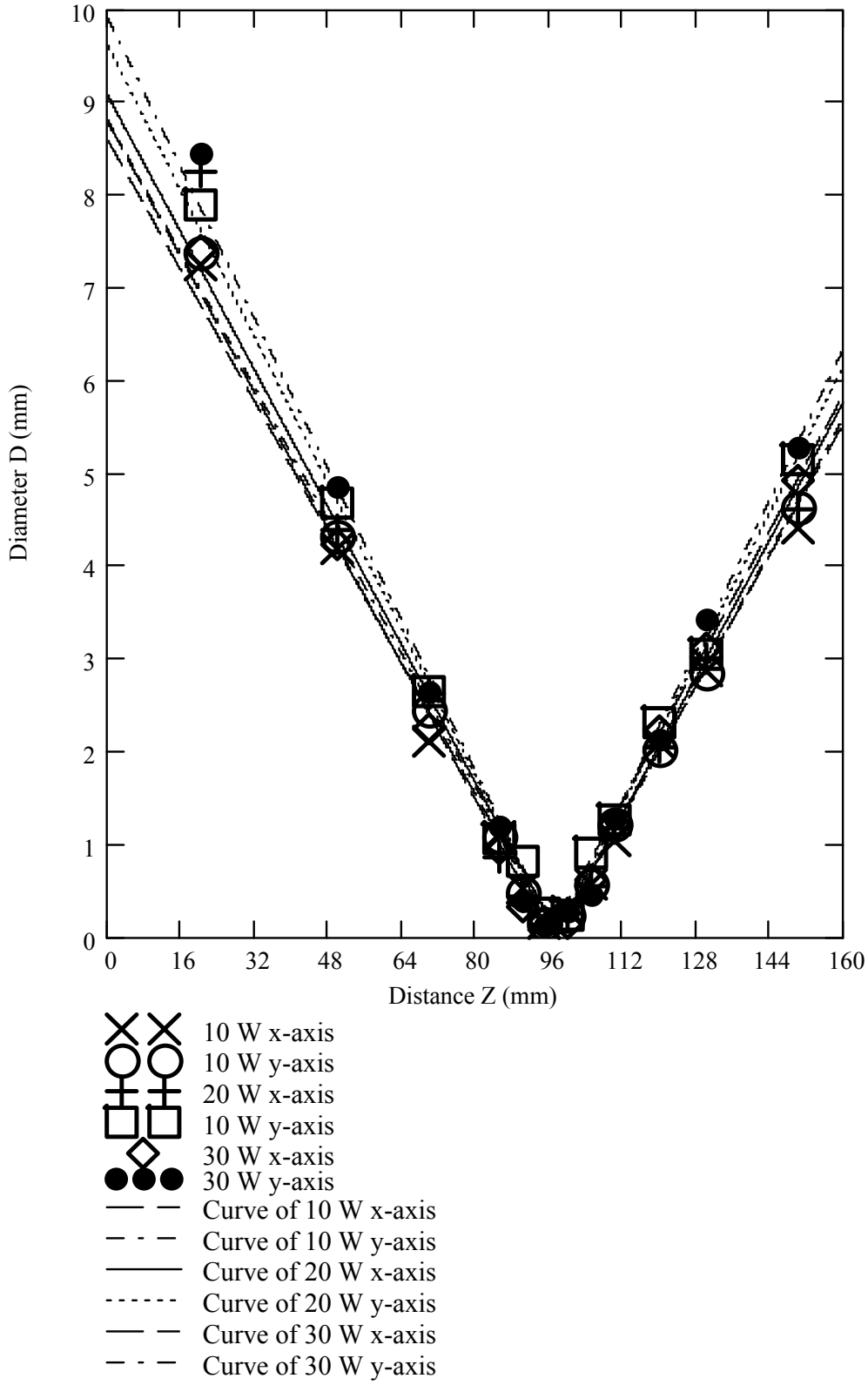

Figure A5.1 - Experimental data with fitted curves along the propagation direction

A5.4.5 - Theoretical Calculation of Beam Diameters at focal point of the lens

$f := 100mm$ Lens focal length

$$D := \begin{pmatrix} 9.026 \\ 8.698 \\ 8.574 \\ 9.353 \\ 8.691 \\ 9.937 \end{pmatrix} mm$$ Beam Diameters on the lens

$$d_j := \left[\frac{4}{\pi} \cdot \frac{\lambda \cdot f}{D_j} \cdot \left(M_j\right)^2 \right] + 0.0286 \frac{\left(D_j\right)^3}{f^2}$$

$$d = \begin{pmatrix} 0.167 \\ 0.16 \\ 0.179 \\ 0.152 \\ 0.163 \\ 0.153 \end{pmatrix} mm$$

$$difference_j := \frac{\left| \frac{d_j}{mm} - I_{1,j} \right|}{\frac{d_j}{mm}} \cdot 100$$

$$difference_j = \begin{pmatrix} 0.9 \\ 4.5 \\ 8.5 \\ 6.5 \\ 6.1 \\ 4 \end{pmatrix}$$

A5.4.6 - Focal Depth

$$z_{f_j} := \left(\left| I_{2,j} - root\left(\omega\left(x, I_{1,j}, I_{2,j}, I_{3,j}\right) - \sqrt{1.05}, I_{1,j}, x, I_{2,j}, 160\right)\right| + \left| I_{2,j} - root\left(\omega\left(x, I_{1,j}, I_{2,j}, I_{3,j}\right) - \sqrt{1.05}, I_{1,j}, x, 50, I_{2,j}\right)\right| \right) mm$$

$$z_f = \begin{pmatrix} 0.85 \\ 0.76 \\ 0.79 \\ 0.65 \\ 0.75 \\ 0.65 \end{pmatrix} mm$$

APPENDIX VI

BEAM DELIVERY UNIT and NOZLE DRAWING

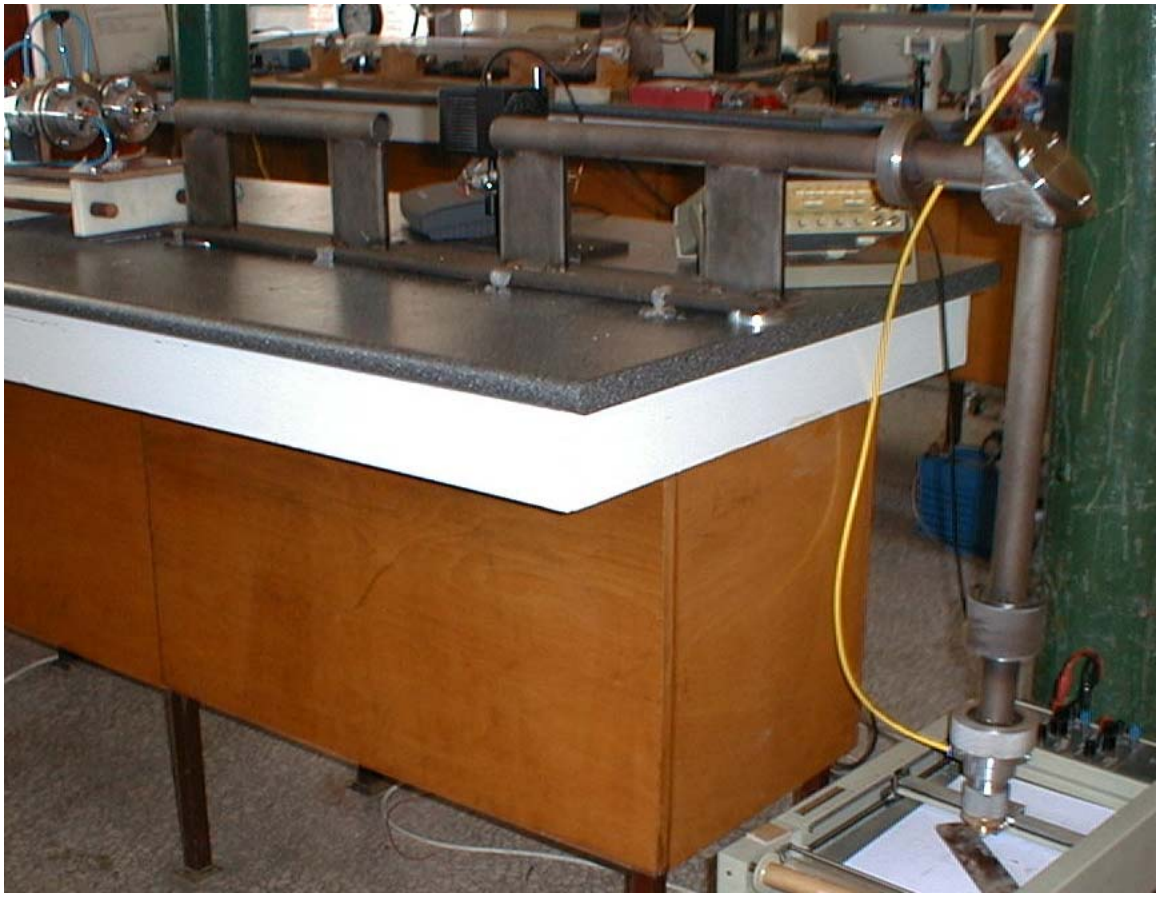

Figure A6.1 – Beam delivery unit

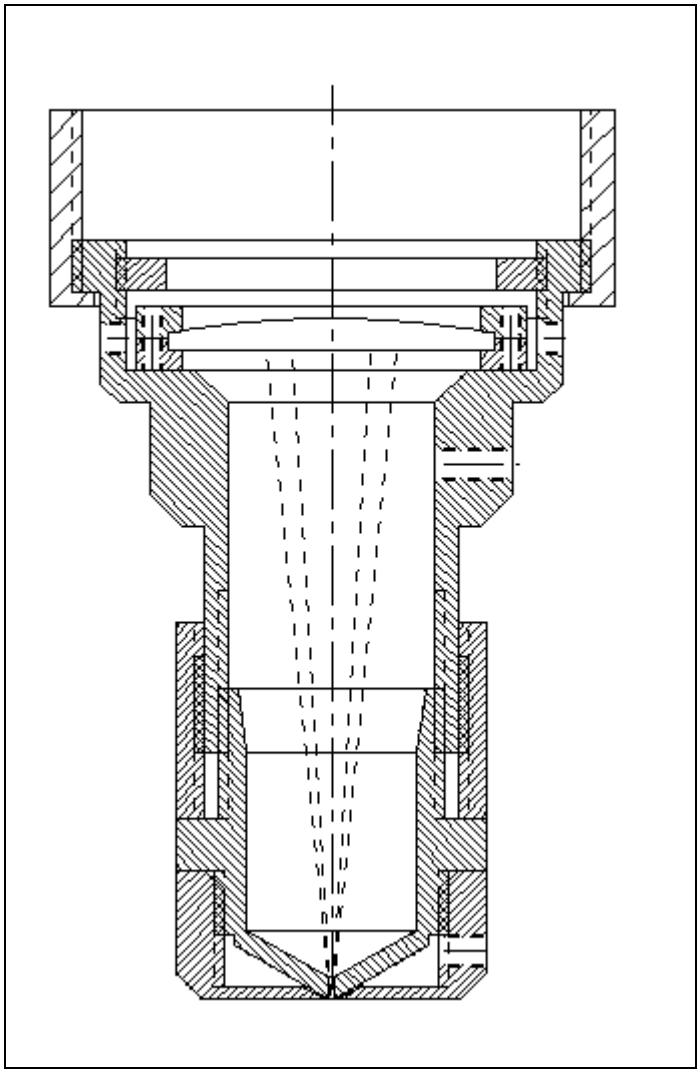

Figure A6.2 - Laser beam focusing head and nozzle